Effect of a Thio Group on Simplified Analogs of Bleomycin

THOMAS J. LOMIS[a,b], JENNIFER MARTIN[b], BARBARA McCLOSKEY[a], SONGSHENG ZHANG[c], SHIRIN SIDDIQUI[c], REX E. SHEPHERD[c]* and JEROME F. SIUDA[a,b]*

Departments of Pharmaceutical Sciences[a] and Medicinal Chemistry[b], School of Pharmacy and Department of Chemistry[c], University of Pittsburgh, Pittsburgh, PA 15261, U.S.A.

(Received July 8, 1988)

Abstract

Two new series of ligands, SAPH (**1**–**3**) and DAPHS (**4**–**6**) related to the metal chelating portion of the anti-tumor drug bleomycin (BLM) have been synthesized and evaluated. These series differ from the related simplified models, PYML and AMPHIS by modifications of the primary amine of PYML and AMPHIS to a thio functionality (–SR) (R = CH_3, **1**; R = $CH_2C_6H_4OCH_3$, **2**; R = H, **3**) in the SAPH (**1**–**3**) series and by the additional change of the secondary amino functionality of SAPH to an amido unit in the DAPHS (**4**–**6**) compounds. SAPH (**1**–**3**) and DAPHS (**4**–**6**) are, therefore, potentially five-coordinate N_4S donor ligands possessing imidazole, amide, pyridine, amine, and sulfhydryl moieties for SAPH-3 and imidazole, amide, pyridine, amide, and sulfhydryl for DAPHS-6. One:one metal:ligand complexes were prepared with Cu^{II}, Fe^{II} and Fe^{III}. Frozen glass ESR spectra and electronic spectra at room temperature of the Cu^{II} complexes show that the resultant coordination geometry and choice of ligand donor set is strongly influenced by pH. Cu^{II}(SAPH-3) exhibits imidazole, pyridine, amine and sulfhydryl (N_3S) coordination in a trigonal bipyramidal complex at 2.80. The coordination changes to imidazole, deprotonated amide, pyridine and amine (N_4) at pH $\geqslant$ 5.80; the ESR spectra require rhombically distorted square-planar coordination similar to Cu^{II}(AMPHIS) and Cu^{II}(BLM) in this range. Cu^{II}(DAPHS-6) exhibits ESR spectra indicative of 2N (imidazole, pyridine), 3N (imidazole, first amide, pyridine) and 4N (imidazole, pyridine, and both amides) coordination at pHs of 3.18, 5.62 and 8.00, respectively. Sulfhydryl coordination for Fe^{III}(SAPH-3) is indicated by the presence of charge transfer bands (>400 nm) which are absent for the SCH_3 analog, Fe^{III}(SAPH-1), and by the electrochemical behavior of Fe^{II}(SAPH-3) above pH 6.9 where N_4S coordination is observed. Fe^{II}(SAPH-1) reacts with molecular O_2 but possesses one-tenth the activity of Fe^{II}(AMPHIS), in forming HO· or HO_2· radicals which escape the solvent cage of the Fe^{III} complex for trapping by DMPO or PBN spin-trap scavengers. Fe^{II}(SAPH-3) shows no free HO· trappable by DMPO during autoxidation, indicative of $2e^-$ reduction steps. Fe^{II}(SAPH-3) exhibits no reversible $1e^-$ electrochemical wave from –0.64 to +1.24 V for forms having sulfhydryl coordination, but the same complex reacts rapidly with $2e^-$ chemical oxidants (O_2, H_2O_2, Ru^{IV}). Diamide analogs (DAPHS) also lack HO· or O_2^- generating activity.

Introduction

Bleomycin (BLM) is a clinically useful anti-cancer drug composed of a mixture of glycoproteins of related structure [1]. The drug is employed in the treatment of Hodgkin's lymphoma, carcinomas of the head, skin and neck and tumors of the testis and ovaries. A variety of approaches have been employed to determine the molecular mechanism of action [2] as well as to analyze the factors contributing to the pulmonary toxicity of the drug [3]. The chemistry of BLM has been recently reviewed by Hecht [4].

Bleomycins possess two significant structural features: a DNA binding component which differs in the bithiazole region and cationic terminus of the molecule of each BLM, and a coordination area which chelates metals by the same functional groups for all BLMs. Upon chelation of reducing metals such as Fe(II), Cu(I) and Co(II), the coordination center of the drug then binds dioxygen and reduces the molecule to an 'activated' species of oxygen, which then cleaves the proximately bound DNA. The activated oxygen may be in the form of several types of free or bound radicals or ion radicals (O_2^-, HO_2·, O-atom and HO·) [2d, 5] which in turn may also contribute to damage in the lung [3]. Overall, the chelation of transition metals, binding and reduction of dioxygen by BLM resembles the enzymology of peroxidase enzymes, including cytochrome P-450 [4–6].

A number of model compounds related to BLM have been synthesized in order to study the structural characteristics required in the mechanism of action. Among the simplified analogs of BLM are PYML [7] and AMPHIS [8]. Both of these substances

*Authors to whom correspondence should be addressed.

0020-1693/89/$3.50

bind $Fe^{II/III}$ and $Cu^{I/II}$, mediate the formation of active oxygen and thus serve as simplified models for the chelating portion of BLM. A synthetic structural analog of the BLM metal binding region, $Cu^{II}(PMA)^+$, was recently described by Brown *et al.* [9]. The participating ligands in the chelate of the models consist of five nitrogen donors, *i.e.* imidazole, amide, pyridine (or pyrimidine in PMA^-), secondary amine and primary amine. Based primarily on the studies of Sugiura *et al.* [7] and Henichart *et al.* [8] the illustrated structure serves as a representative chelate of PYML and AMPHIS. This coordination geometry is found for $Cu^{II}(PMA)^+$ [9]. With four nitrogen

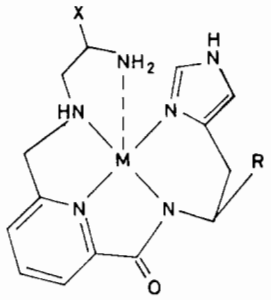

PYML: X = $CONH_2$, R = CO_2CH_3 or CO_2H

AMPHIS: X = H, R = CO_2CH_3

donors participating in-plane and the primary amine in an apical position, a sixth ligand may participate in the second axial position. This remaining site may be occupied by O_2 which eventually becomes reduced to a more chemically reactive species. The primary amino group which has been postulated to participate at an axial position of the $Fe^{II}(BLM)$ complex, plays an important role for generation of active oxygen. Acetylation of this amine in bleomycin results in a substance devoid of oxygenation activity [10]. One of our chief goals in this research was to study the effect of replacing the amino function with a bioisosteric sulfhydryl group. Cytochrome P-450 possesses a thiol functionality in an axial position of an iron-octahedral complex. A sulfhydryl group built into the bleomycin model enables comparisons with both the drug and the enzyme. Replacement of an $-NH_2$ by SH, is a well established approach in medicinal chemistry for studying structure–activity relationships.

In light of the above discussion, the syntheses of compounds **1–3** (SAPH series) and **4–6** (DAPHS series) were undertaken in order to determine both structural characteristics and ability to generate activated oxygen. We chose not to incorporate the terminal amide group of PYML nor the ester found in PYML or AMPHIS as these groups do not appear to participate as donors to the metal. If the thiol (–SH) or thiolate ($-S^-$) moieties bind to the metal, then differences might be expected when comparing **1** *versus* **3**. In addition to exploring the effect of $-NH_2$ *versus*

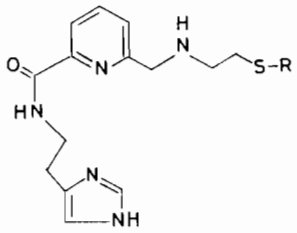

SAPH

1 R = Me

2 R = MBz

3 R = H

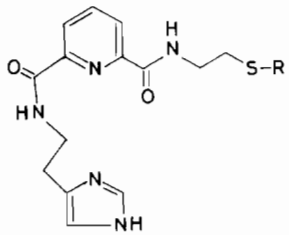

DAPHS

4 R = Me

5 R = MBz

6 R = H

–SH and –SH *versus* –SMe, compounds **4–6** were prepared to determine what changes would occur in further altering the ligand characteristics of the model analogs. Replacement of the secondary amino by the amide alters both the stereochemistry (sp^3 *versus* sp^2) and the donating properties of the ligand.

Results and Discussion

Synthetic Approach

Scheme 1 illustrates the syntheses of compounds **1–3** (SAPH series) from the known aldehyde **7**. Reductive amination with the cysteamine analog $N_2NCH_2CH_2SR$ in the presence of sodium cyanoborohydride [11] afforded good yields of the amino esters **8** or **9**. Reaction of histamine with **8** or **9** at

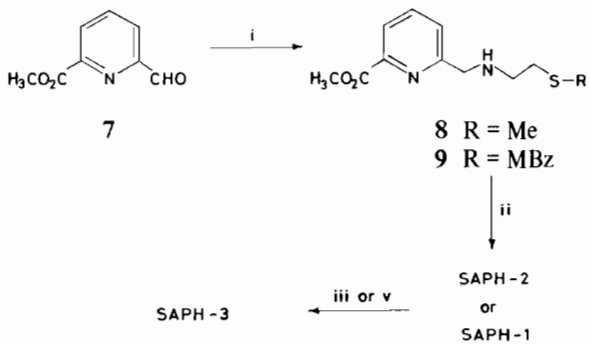

7

8 R = Me

9 R = MBz

Scheme 1. For (i), (ii), (iii) or (iv) see legend to Scheme 2.

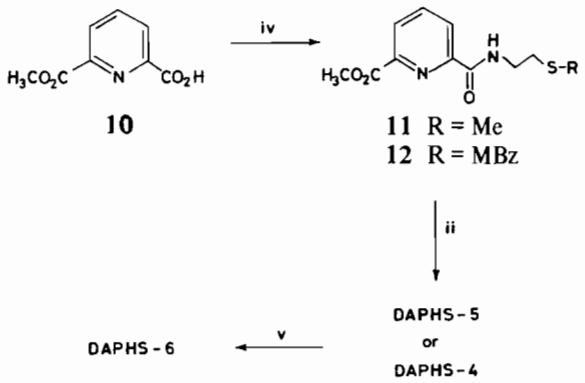

Scheme 2. (i) $H_2NCH_2CH_2SR$, $NaCNBH_3$/MeOH, pH 6. (ii) Histamine/MeOH. (iii) HF, 0 °C. (iv) $H_2NCH_2CH_2SR$, DCC, HOBT/DMF or dioxane-CH_2Cl_2. (v) F_3CCO_2H, 85–90 °C.

room temperature for several days proceeded smoothly to give **1** and **2**, respectively. With the eventual aim of producing a free thiol moiety *viz.* **3** (or **6**) the 4-methoxybenzyl (MBz) derivative was chosen to protect the thiol from forming a thiazolidine ring during the reductive amination reaction [12]. The MBz group could be readily removed in the last reaction steps without affecting the other functional groups in the final products. Compound **2** was then treated with either HF [12, 13] at 0 °C or F_3CCO_2H at 85–90 °C to afford **3** in excellent yield. Compound **3** was isolated as the trihydrochloride as indicated by NMR chemical shift data. Attempts to shorten the route to **1** by methylation of **3** were unsuccessful.

The preparation of diamide analogs **4**–**6** (DAPHS series) are described in Scheme 2. Condensation of the acid–ester **10**, with the appropriate derivatized cysteamine provided the intermediate amide esters **11** or **12**. Similar to the procedure in Scheme 1, reaction with histamine gave the desired diamides **4** or **5**. Removal of the methoxybenzyl group from **4** was easily accomplished using F_3CCO_2H yielding **6** in quantitative yield. The majority of new compounds were oils which strongly retained water or even volatile solvents, e.g. alcohols, ether, etc. Salts of the final products were prepared in most cases and were utilized in the spectroscopic evaluations described below.

Cu(II) Complexes of the SAPH and DAPHS Series (1–3 and 4–6)

Cu(II) derivatives of the ligand series SAPH (**1**–**3**) and DAPHS (**4**–**6**) were prepared at 1:1 stoichiometry as determined by spectrophotometric titration [14]. No evidence for a 2:1 interfering complex was observed. The extent of chelation by the ligands was examined as a function of pH by obtaining ESR spectra of the complexes in 50:50 DMSO:H_2O frozen glasses at 123 K*. Complementary ligand field spectra were recorded between 800 and 350 nm at room temperature. The spin Hamiltonian ESR parameters and the d–d transition spectral maxima are recorded as a function of pH in Table 1.

The intent of the study of the Cu(II) derivatives of **1**–**3** and **4**–**6** was to elucidate how the SAPH and DAPHS series coordinate to Cu(II) as a comparison with available data for the BLM, PYML and AMPHIS Cu(II) complexes [15]. PYML and AMPHIS have not been studied over a wide range of pH and the study of BLM is incomplete at low pH [16]. Cu(II) complexes may adopt a variety of coordination geometries which are dependent on the number and type of

*Binuclear Cu(II) species would also be evident by line broadening to a single derivative in the ESR spectra; such broadening was absent.

TABLE 1. Spin Hamiltonian and Ligand Field Parameters for Cu(II) Complexes of the SAPH and DAPHS Series[a]

Cu(II)–Ligand	pH	Type of ESR[b]	max (nm)	$A_{\parallel}$ (G)	$g_{\parallel}$	$g_{\perp}$	$A_{\perp}$ Cu
SAPH-1	3.00	A	567	144	2.20	2.09	
	6.25	RDA	567	130	2.16	2.03	
	8.30	RDA	567	122	2.16	2.01	
SAPH-3	3.00	R-tbp	600, 695sh	140	[c]	2.11	58
	5.80	RDA	570	139	2.15	1.95	
	8.60	RDA	567	144	2.10	1.96	
DAPHS-5	6.70	RDA		242	2.18	1.98	
DAPHS-6	3.80	A	612, 700sh	129	2.36	2.02	
	6.00	R-tbp	598	[c]	[c]	2.16	160
	8.00	RDA	545	200	2.12	2.00	

[a]ESR spectra were obtained in 50:50 volume percent DMSO: water frozen glasses at 123 K; pH adjustment was made at room temperature prior to freezing. [b]A = axial, R-tbp = reserve trigonal bipyramidal, RDA = rhombically distorted axial. [c]Intensity is too low for accurate measurement.

available ligand donors. With multidentate chain-like ligands such as the SAPH and DAPHS series, both pH and stereochemical constraints will be important for the ultimate solution structure of a complex in a given pH regime. The coordination of the deprotonated amide is anticipated only with pH > 6 [17]. The imidazole and pyridine donors are anticipated to be coordinated even in a more acidic region (pH ≈ 3 of this study) while the amine functionality of SAPH (**1**–**3**) is likely to be protonated and removed from coordination in acidic solutions. For example, a crystal structure of a Cu(II) complex possessing a protonated pendant ethylenediamine while retaining coordinated axial pyridine units, two chloride donors and an in-plane amine, has been resolved by Mandel and Douglas [18] for the bis(2-pyridylmethyl)*N*,*N*-ethylenediamine complex which is isolated from acid solutions (pH ≤ 2). Related pH controls on the geometries of the Cu(II) complexes of SAPH and DAPHS have been observed in this work.

Cu(II) complexes commonly are found in geometries of one of the tetragonal forms whose local site symmetries are close to D_{4h} or C_{4v} (Jahn–Teller distorted octahedral, square planar and square pyramidal species and rhombically distorted modifications of these or the trigonal bipyramidal coordination with site symmetry near D_{3h}) [19]. The tetragonal forms exhibit one of several characteristic ESR patterns for Cu(II) complexes which are termed tetragonal, axial or rhombically distorted axial depending upon the extent of splitting of g_{xx}, g_{yy} and g_{zz} transitions [19–21]. The trigonal bipyramidal complexes with a smaller ligand field than D_{4h} or C_{4v} give rise to the reversed ESR pattern in which $g_\perp$ transitions appear at energies either below or overlapping $g_\parallel$ transitions. The electronic transitions for a trigonal bipyramidal complex of the same set of ligand donors also reside lower in energy than those of a tetragonal complex for the same ligand field reasons. Therefore, the d–d transitions will provide supporting evidence for structures which are implicated by an ESR spectrum [19].

A number of solution structural arrangements are possible for the Cu(II) derivatives of **1**–**3** and **4**–**6**. The ligands with terminal sulfhydryl groups, SAPH-3 and DAPHS-6, gave particularly interesting results. In the pH 7 to 8 range, the species share the rhombically distorted axial ESR patterns of PYML and AMPHIS derivatives [8b, 15] but below pH 7 more unique spectra, characteristic of five-coordination, appear which has not been explored for PYML or AMPHIS. The ESR spectrum of Cu^{II}(DAPHS-5) at pH = 6.70 is shown in Fig. 1. Nine N-shf lines (A_N = 15 G) appear on the low-field side of the $g_\perp$ component of a rhombically distorted axial (tetragonal) spectrum. A distorted square-planar geometry with four N donors is required. This implicates two deprotonated amide donors as well as the imidazole and pyridine groups of DAPHS-5.

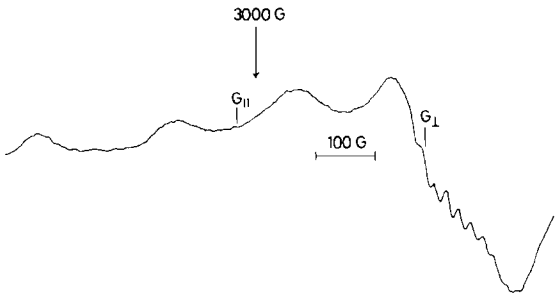

Fig. 1. ESR spectrum of Cu^{II}(DAPHS-5) in Me_2SO/water glass at 123 K: pH = 6.70, 9.088 GHz, 12.5 G m.a., 4×10^3 r.g., 20 mW, 4.0 min scan, 1.0 s time constant, [Cu(II)] complexes = 4.43×10^{-3} M.

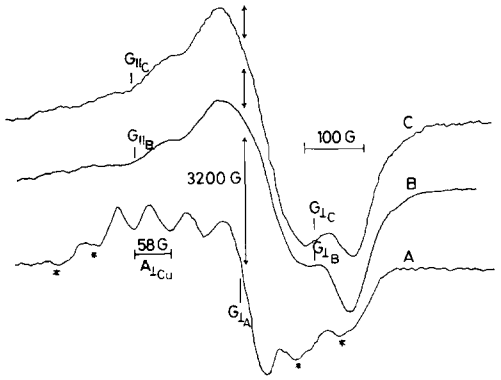

Fig. 2. ESR spectra of Cu^{II}(SAPH-3) in Me_2SO/water glass at 123 K: (A) pH = 2.80, 9.090 GHz, (B) pH = 5.80, 9.008 GHz, (C) pH = 9.70, 9.090 GHz; all other settings as in Fig. 1.

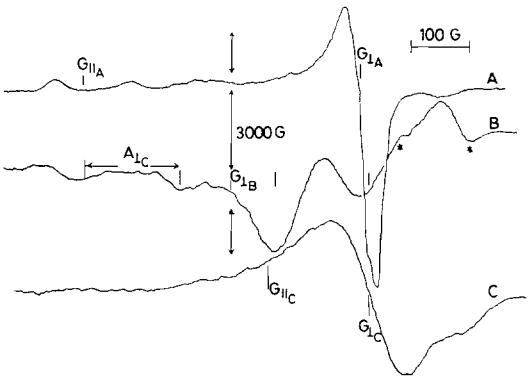

Fig. 3. ESR spectra of Cu^{II}(DAPHS-6) in Me_2SO/water glasses at 123 K: (A) pH = 3.18, 9.090 GHz, 2.5×10^3 r.g. (B) pH = 5.62, 9.088 GHz, 6.3×10^3 r.g. (C) pH = 8.00, 9.09 GHz, 5.0×10^3 r.g.; all other settings as in Fig. 1.

ESR spectra for the Cu(II) complexes of SAPH-3 and DAPHS-6 as a function of pH are shown in Figs. 2 and 3, respectively. Cu(II) complexes of tripeptides and metalloproteins have shown that the Cu(II) will assist the deprotonation of amide hydrogens in the

physiological pH range of 6 to 8 [17, 22]. The influence of amide coordination is observed in the changes in both the ESR and visible spectra of the SAPH-3 and DAPHS-6 complexes; the amide donors of these ligands which are present between the imidazole and pyridine functionalities do not begin to coordinate until the pH is increased to approximately 4.5. The second amide donor in DAPHS-6 becomes coordinated in the vicinity of pH 8.0. The changing structural chelation of Cu^{II}(SAPH-3) is shown in Fig. 2. At low pH (2.80), a reversed ESR pattern is observed with a regular progression of four lines spaced 58 G apart ($A_\perp$ Cu) for the line. A background set of transitions are also observed with $A_\parallel$ spacings of 140 G. These are denoted by (*) on Fig. 2A. As the pH is increased to 5.80 the spectrum changes to a tetragonal pattern (Fig. 2B). These features are retained at higher pH (9.70) with only a slight change in $g_\parallel$. Spectra 2B and 2C are very similar to the one reported by Henichart *et al.* for Cu(AMPHIS) [8]. Concomitant with the changes in the ESR spectra are the changes in the visible spectra of Cu(SAPH-3). A broad double band with maxima at 600 nm and a 695 nm shoulder (pH = 3.0) is replaced with a more symmetric band absorbing at 570 nm (pH = 5.80) followed by a slight shift to 567 nm (pH $\geqslant$ 8.60). The major spectral change occurs where amide deprotonation is common and occurs with a redefinition of a strong ligand field (R-tbp $\rightarrow$ RDA). The smaller spectral shift probably involves deprotonation of an axial H_2O donor; however, reinvolvement of the sulfhydryl group at high pH ($\geqslant$9.70) might also be accommodated by the data. The coordination of the sulfhydryl in the low pH regime is established from a parallel study of the S-CH_3 derivative, SAPH-1, which is described later. Since the related Cu(DAPHS-4) complex also establishes amide coordination in the pH 6 range, the structure of Cu(SAPH-3) is assigned as shown below.

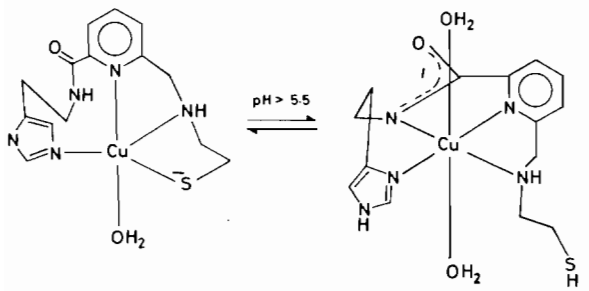

The $g_\perp$ region of the Cu(SAPH-1) complex is shown in Fig. 4. The S-CH_3 derivative shows a severely rhombic ESR pattern at pH = 6.25 which changes to a more regular RDA spectrum at pH = 8.30. An alternate interpretation may be made, that the features change due to the absence of anomalous lines at high pH [21]. In either case, a structural change is

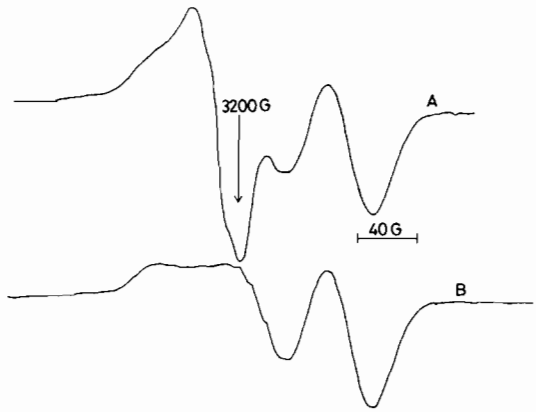

Fig. 4. ESR spectra in the $g_\perp$ region of Cu^{II}(SAPH-1) in Me_2SO/water glasses at 123 K: (A) pH = 6.25, 9.089 GHz, 2.0×10^3 r.g. (B) pH = 8.30, 9.085 GHz, 2.0×10^3 r.g.; all other settings as in Fig. 1.

implied. Spectra of the same two types are observed for the S-MBz derivative, Cu(SAPH-2), at pH 3.0 and 8.80, respectively. The pH 8.30 spectrum of Cu(SAPH-1) is similar to Cu(SAPH-3), at pH = 8.60. Under these conditions both Cu(SAPH-1) and Cu(SAPH-3) have a matching visible spectrum indicating the same coordination at pH 8.3. The poor donor ability of S–CH_3 compared to water or DMSO assures that the S–CH_3 group is pendant; therefore, the –SH group must also be free at pH 8.3 as indicated previously. The additional distortion exhibited in Fig. 4A for Cu(SAPH-1) at pH = 6.25, suggests three strong donors which do not adopt a strictly planar arrangement. This may be produced by a minor buckling of chelate rings formed by imidazole, pyridine and amine donors. This ESR pattern is intermediate between normal RDA and R-tbp spectra; thus the complex has a structure intermediate between tetragonal and trigonal bipyramidal limiting forms. This out-of-plane distortion or anomalous line feature is removed when amide coordination forces a more regular in-plane ligand field (Fig. 4B). In addition, the ESR pattern of Cu(SAPH-1) at pH 6.25 (Fig. 4A) is sufficiently different from the reversed trigonal bipyramidal coordination exhibited by Cu(SAPH-3) at pH 2.80 to require that a different total number of donors is bound for Cu(SAPH-3) at pH = 2.80 and Cu(SAPH-1) at pH = 6.25. Yet both would possess the imidazole, pyridine and amine coordination. Since it is very unlikely that the S–CH_3 donor can compete with water or DMSO for coordination at Cu(II), and the remainder of the ligand structure would be identical for SAPH-1 and SAPH-3, we conclude that the sulfhydryl group of SAPH-3 is coordinated at pH 3 to 5 as shown above. This conclusion is further supported by the differences observed in the d–d transitions at 567 nm for Cu^{II}(SAPH-1) *versus* 600 nm for Cu^{II}(SAPH-3), although both

complexes should have the same three N-donors. Presence of the sulfhydryl group coordinated to Cu(II) should weaken the ligand field due to the π-donor ability of an RS^- group, compatible with the lower energy transition for Cu^{II}(SAPH-3).

When the deprotonated amide unit forces the change in coordination from trigonal bipyramidal to rhombically distorted axial at pH $\geqslant$ 5.8 the pendant sulfhydryl will become protonated by solvent. A similar observation with protonation of a displaced sulfhydryl group even though the pH is increased to coordinate another ligand donor, has been described for a copper redox metalloprotein of the cytochrome oxidase complex [23].

Related changes for the Cu(II)(DAPHS-6) complex are shown in Figs. 3A–3C. The axial ESR spectrum 3A at pH 3.18 shows very weak N-shf suggesting two N-donors which are most probably the imidazole and pyridine moieties. This species converts at about pH 5.6 to a complex of trigonal bipyramidal coordination and the relevant ESR spectrum 3B is of the reversed type. A related ESR pattern was observed for $Cu^{II}(IMEPH)^{2+}$ where 7 N-shf lines are also detectable, indicative of three N donors in a trigonal bipyramid [24]. The $Cu^{II}(IMEPH)^{2+}$ complex shares the identical coordination chain linkage of DAPHS-6 up through the pyridine donor moiety. At pH 8.00, a rhombically distorted tetragonal spectrum is obtained (3C). These various changes are consistent with imidazole and pyridine donation at pH 3.80 which changes to three N donors coordinated at 6.00 (first amide coordination) and four N donors at 8.00 (second amide) as shown below. These major changes in structure are also supported by a progressively stronger ligand field producing d–d transition maxima at 612 and 700 nm for the axial complex with 2N donors, 598 nm for the trigonal bipyramidal species with 3N donors and 545 nm when 4N donors (two coordinated deprotonated amides) are implicated by ESR.

The parameters of several Cu(II) complexes of the present series are compared to literature values for Cu(II) derivatives of bleomycin (BLM), AMPHIS, PYML, and PMA^- in Table 2. There are minor differences between the present series and those of the

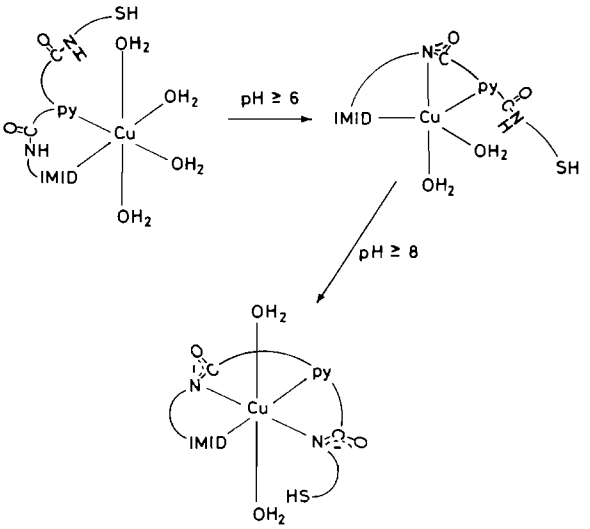

other complexes which may be due to the absence of a common frozen glass medium for all of the data. Overall the agreement is reasonable. The Cu(SAPH-3) and Cu(DAPHS-6) species at pH = 8 will lack an axial N donor which is present in BLM, AMPHIS, PYML and PMA^-.

This is observed with a greater variability in $A_{\|}$ for the SAPH and DAPHS series than in the related cases where the axial coordination of an N donor is assured. $A_{\|}$ is seen to be nearly constant at 180 G for the N_5 cases. The average splitting between $g_{\|}$ and $g_{\perp}$ is also slightly smaller, being *ca.* 85% for SAPH and DAPHS of the systems having five N donors.

Fe(II) and Fe(III) Complexes of SAPH-1 and SAPH-3

Samples of Fe^{II}(SAPH-1) and Fe^{II}(SAPH-3) (2.0×10^{-3} M) were prepared by addition of limiting amounts of $Fe(NH_4)_2(SO_4)_2 \cdot 6H_2O$ to the respective ligand solution (3.0×10^{-3} M) under Ar. The solutions appeared colorless below pH = 3.5, but changed to give a bright yellow solution for Fe^{II}(SAPH-1) and a reddish-orange solution for Fe^{II}(SAPH-3) above pH 5.7. The intensity appeared to be fully developed at pH 7, but again became more red in the pH $\geqslant$ 9 range. The spectra from 800 to 350 nm and the related first pH change are similar to those observed

TABLE 2. ESR Data for Cu^{II} BLM and Simplified BLM Models

Complex	$A_{\|}$ (G)	$g_{\|}$	$g_{\perp}$	Reference
Cu(SAPH-3) (pH = 8.6)	144	2.10	1.96	this work
Cu(DAPHS-6) (pH = 8.0)	200	2.12	2.00	this work
Cu(SAPH-1) (pH = 8.3)	122	2.16	2.01	this work
Cu(BLM)	183	2.21	2.06	15
Cu(AMPHIS)	177	2.21	2.05	8
Cu(PYML)	179	2.21	2.05	15
$Cu(PMA)^+$	184	2.210	2.052	9

with Fe^{II}(BLM) as a control. Appearance of the red–orange colors of the d–d type (with an LMCT contribution causing higher extinction coefficients) indicates the amide deprotonation with at least the N_4 in-plane donor set for SAPH-1 or SAPH-3. The high-spin d^6 configuration should then possess a weak LMCT transition involving the Fe^{II}–amide functionality. The spectra of the Fe^{II} complexes are similar in the visible region with respective LMCT transition maxima and extinction coefficients as follows: Fe^{II}(BLM), 476 nm, 380 M^{-1} cm^{-1}; Fe^{II}(PYML), 465 nm, 300 M^{-1} cm^{-1}; Fe^{II}(SAPH-3), 475 nm, 190 M^{-1} cm^{-1} [15, 27]. The pH dependent spectral changes which are observed for Fe^{II}(SAPH-3) and Fe^{II}(SAPH-2) are related to those identified previously for Fe^{II}(HAPH) [25]. The changes in the solution species as indicated by five color changes for the Fe^{II}(SAPH-3) complex and four color changes for Fe^{II}(SAPH-2) in the pH range of 3 to 9 suggest the following species in solution as a function of pH (Scheme 3). An interpretation of the coordination geometries and electrochemical behavior for Fe^{II}(SAPH-3) is supported by prior studies of the Fe^{II}(HAP) and Fe^{II}(HAPH) complexes [25]. The electrochemical behavior for the Fe^{II}(HAP) and Fe^{II}(HAPH) complexes is quasi-reversible and allows proper assignment of the number and type of N donors for the Fe^{II}(HAPH) complex [25]. The ligands HAP and HAPH are similar to the SAPH series as shown below.

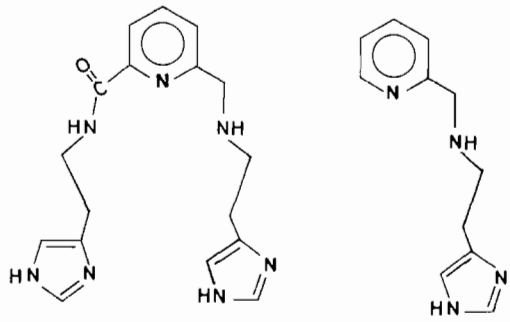

The solution colors and suggested ligand field donor set compatible with the pH-dependent changes are listed in Table 3. Based on the color changes observed for the Fe^{II}(SAPH-3) complex, we estimate the sulfhydryl pK_a in species **2A** to be *ca.* 4.0, the amide proton with coordinated sulfhydryl in **2B′** of *ca.* 5.7, while the amide with the dissociated sulfhydryl group (**2B**) at 6.5. The latter form (**2B**) has an identical pK_a observed for species **1B** of the Fe^{II}(HAPH) complex of 6.50 ± 0.05 [25]. The sulfhydryl pK_a of species **2B** appears to be *ca.* 7.5 while the analogous deprotonation of the pendant imidazolium moiety of Fe^{II}(HAPH) occurs at *ca.* 8.0 [25]. Kimura *et al.* [26] have recently prepared the related ligands L_1 and L_2 (see p. 106).

TABLE 3. pH-Dependent Color Changes of $Fe^{II}L$ Complexes[a]

pH	Fe^{II}(SAPH-3)	Fe^{II}(SAPH-2)	Fe^{II}(HAPH)[b]	Fe^{II}(HAP)[b]
2.10			dirty pink	
3.00	light yellow			
4.10			dusty rose, N_4 (no amide)	
4.87	yellow–orange, N_3S^-			
5.01				light yellow, N_3O_3
5.29		colorless		
5.74	light pink–orange, N_4S^- (no dep. amide)		orange, N_4 (dep. amide)	
6.01				
6.53	orange–pink			
6.86		pale yellow, N_4(SR)		
6.94	orange–red			
7.00	reddish-orange, N_4S (dep. amide)		orange, N_4 (dep. amide)	
7.33				
7.71		yellow–orange, N_4(SR) (dep. amide)		
8.10			dark orange, N_5 (both imidazoles)	
8.13		orange, $N_4(SR)(OH^-)$		
8.20	reddish-orange			yellow, $N_3(OH^-)$
8.70	reddish-brown, $N_4(OH^-)$		reddish-brown, $N_4(OH^-)$	

[a] M = 0.10 $NaClO_4$, T = 22 °C. [b] Ref. 25.

These ligands are quite similar to AMPHIS [8]. Kimura *et al.* [26] report species corresponding to **1B** and **1C** or **2B** and **2C** for the L_2 case. Presumably the amide adjacent to the terminal amine lowers the pK_a of the terminal amine to promote competitive binding by Fe^{II} *versus* H^+ for L_2 in the physiological range. Therefore Fe^{II}(HAPH) [25], Fe^{II}(SAPH-3) and $Fe^{II}(L_2)$ [26] all exhibit species documented for structures of the $N_4(OH_2)$ and N_4(axial base) coordination which changes in the pH 6.5 to 8.5 range.

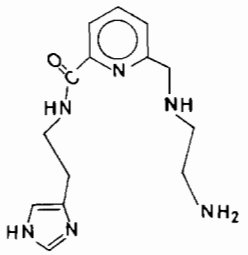

L_1

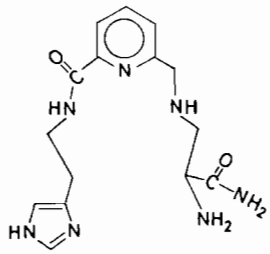

L_2

The behavior of Fe^{II}(HAPH) [25] and $Fe^{II}(L_2)$ [26] in this range was crucial to the assignments of coordination changes given in Scheme 3. The uniquely different electrochemical behavior of Fe^{II}(SAPH-2) and Fe^{II}(SAPH-3) is also important in these assignments. Taking the orange species of Fe^{II}(HAPH) which has an imidazole, deprotonated amide, pyridine and secondary amine in-plane donors at pH ~ 7.0 as a basis, the additional reddish contribution in the Fe^{II}-(SAPH-3) complexes is indicative of sulfhydryl coordination which allows for additional LMCT bands due to the π-donating sulfhydryl anion. The Fe^{II}-(SAPH-2) species at similar pH are more yellow; this is compatible with the poorer π-donating thio ether in competitive coordination with water in the fifth position. All species of Fe^{II}(SAPH-3), Fe^{II}(SAPH-2) and Fe^{II}(HAPH) exhibit a change to reddish-brown or dark orange at pH ~ 9.0 indicative of hydroxide coordination. Demetallation occurs above pH 10.

Admission of O_2 to Fe^{II}(SAPH-1) yields a yellow solution which demetallates as $Fe(OH)_3$, hydrated Fe_2O_3, in about 25 min. The hydrated Fe_2O_3 was isolated and characterized by infrared against an authentic sample. Addition of O_2 changes Fe^{II}-(SAPH-3) in 10 s to a yellow–green solution, followed by olive green at 15 s, yellow at 20 s, and then a slow demetallation forming $Fe(OH)_3$ in 10 min at pH 8 to 9, or 30 min at pH 11.

Authentic Fe^{III}(SAPH-3) prepared under Ar showed that the Fe^{III} complex is metastable at pH = 10.3; demetallation occurred with $t_{1/2}$ = 20 min. The Fe^{II}(SAPH-3)/O_2 solution after 20 s has the same spectral features as Fe^{III}(SAPH-3) prepared via

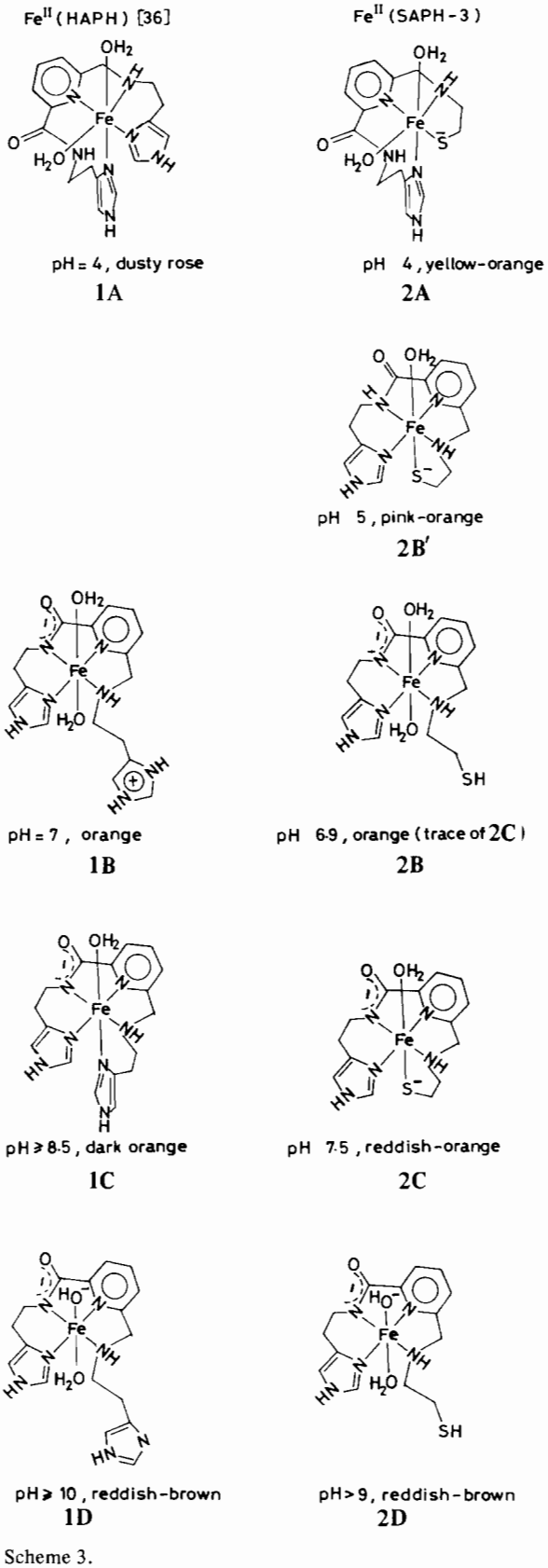

Scheme 3.

$Fe(NO_3)_3$ solution and adjusted to pH = 8. It is known from substitution reactions with polyamines that reattachment of a dissociating base chain is favored unless reformation is blocked by protonation of the leaving group or hydrolysis of the metal center [28]. These studies suggest that the slow demetallation reactions of Fe^{III}(SAPH-1) and Fe^{III}(SAPH-3) probably occur with a rate limiting rupture of the Fe(III)–pyridine-N bond, followed by rapid loss of the hydrolyzed Fe(III) center.

The slower rate at high pH for Fe^{III}(SAPH-3) demetallation suggests additional coordination of the sulfhydryl group which slows the kinetic aspects of the dissociation, but not the thermodynamic favorability of $Fe(OH)_3$ formation. A spectrophotometric titration of Fe^{III}(SAPH-3) also implicates sulfhydryl coordination as described in a subsequent section.

The presence of the greenish intermediate in the autoxidation of Fe^{II}(SAPH-3) may be explained by a bound peroxo complex which has an LMCT transition ($O_2H \rightarrow Fe^{III}$) at *ca.* 700 nm for the transient species or oxidation of the thiolate group. Spin trapping studies indicate the absence of trappable oxygen reduction radical products (O_2^-, HO·) as described later; this is compatible with immediate formation of bound peroxo species by a $2e^-$ path. However a similar intermediate is observed with Ru^{IV} as the oxidant (see below).

Electrochemical Studies of Fe^{II}(SAPH-series) Complexes

The electrochemical behavior of Fe^{II}(SAPH-1), Fe^{II}(SAPH-2) and Fe^{II}(SAPH-3) were evaluated at a glassy carbon electrode *versus* an SCE reference by means of the differential pulse (DP) procedure at 5 mV/s sweep and a 50 mV pulse and by cyclic voltammetry (CV) at 50, 100 and 200 mV/s. The solutions were scanned from –0.56 to +1.24 V *versus* NHE. Fe^{II}(SAPH-1) exhibits its wave at +0.102 V *versus* NHE with a width of 80 mV similar to Fe^{II}-BLM (E° is +0.13 V *versus* NHE) [15], but Fe^{II}-(SAPH-3) exhibited a positive shift to 0.22 V *versus* NHE. It was shown by CV studies that this species is species **2B′** as axial coordination by sulfhydryl and the amide rendered the complex **2C** electrochemically inactive (proven below).

The cyclic voltammetric study of the Fe^{II}(SAPH-2) complex at $\mu = 0.10$ $NaClO_4$, $T = 22$ °C is shown in Fig. 5. The free ligand was shown to be electrochemically silent up to an irreversible oxidation at *ca.* +1.14 V (curve 5A). 2.0 M CH_3OH is present in solution to achieve solubility of the free SAPH-2 ligand at 6.69×10^{-3} M. Addition of $Fe(NH_4)_2(SO_4)_2 \cdot 6H_2O$ and adjustment to pH = 6.94 yielded the cyclic voltammograms of 6.60×10^{-3} M Fe^{II}(SAPH-2) in Fig. 5C. Curve 5C-1 shows the scan at 50 mV/s. The dotted curve 5C-2 shows the fourth repetitive scan at 288 s after scan 5C-1. The dashed curve 5C-3 was obtained

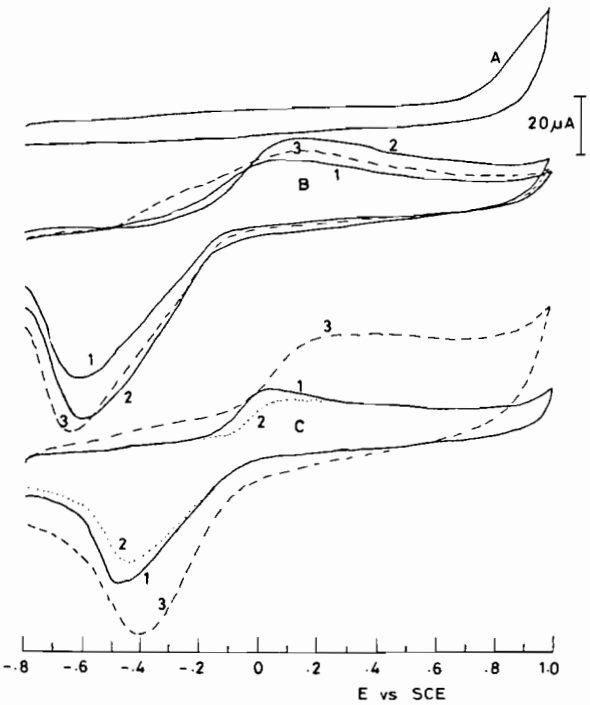

Fig. 5. Cyclic voltammograms of Fe^{II}(SAPH-2) system: (A) SAPH-2 free ligand at 6.67×10^{-3} M, pH = 7.0. (B) Fe^{II}-(SAPH-2) at 6.60×10^{-3} M, pH = 7.71, curve 1, 100 mV/s; curve 2, 200 mV/s; curve 3 restirred and scanned at 200 mV/s. (C) Fe^{II}(SAPH-2), pH = 6.94, curve 1, 50 mV/s; curve 2, fourth scan at 50 mV/s; curve 3, 200 mV/s; SCE reference.

at 200 mV/s. These data implicate a very irreversible wave at *ca.* 0.28 V for the pale yellow form of Fe^{II}-(SAPH-2) and that demetallation of the Fe^{III}(SAPH-2) complex results in a decrease in signal amplitude as in curve 5C-2. The faster 200 mV/s sweep rate shows increasing irreversible character in the oxidation wave. The important result of this study is that curve 5C-1 is identical to the first pH = 5.90 wave for Fe^{II}(SAPH-3) in Fig. 7B; the meaning of this fact will be discussed below. The data at pH = 7.71 for Fe^{II}(SAPH-2) is given in Fig. 5B. The initial scans and decrease in amplitude at 100 and 200 mV/s are similar in kinetic behavior to the data at pH = 6.94, however the color change to yellow–orange implicates the amide deprotonated form of SAPH-2 for the species at pH = 7.71. This is further supported by a negative shift of 0.25 V for the reduction wave relative to the pale yellow (pH = 6.94) form. Unusual behavior for Fe^{II}(SAPH-2) was observed during 50 mV/s repetitive scans in the pH range of 7.71 to 8.50. The pH 7.71 data is shown in Fig. 6. The first scan of Fig. 6C is the same as Fig. 5B. With each subsequent cycle, which requires 72 s at 50 mV/s, a growth of a new species with two oxidation waves and two highly irreversible complementary reduction waves grows in with time. The solution appears

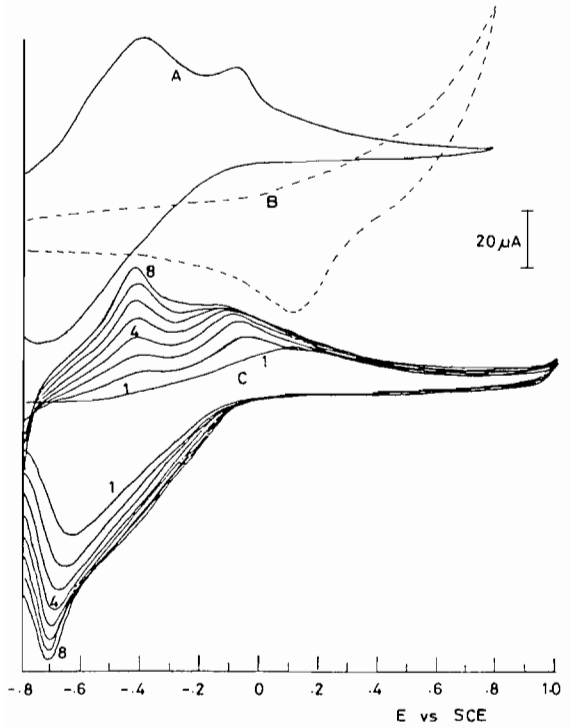

Fig. 6. Polymeric iron cyclic voltammogram: (A) $[Fe(H_2O)_6^{2+}]_i = 6.60 \times 10^{-3}$ M, pH = 8.23, $Fe(OH)_2$ precipitate present; (B) $[Fe(H_2O)_6^{2+}]_i = 6.60 \times 10^{-3}$ M, pH = 6.72, no precipitation; (C) $[Fe(SAPH\text{-}2)]_i = 6.60 \times 10^{-3}$ M, pH = 7.71, scans 1–8 at 50 mV/s; SCE reference.

yellow–orange and no precipitation was detected. The precipitation effect would produce a current decrease in Fig. 6C which is not observed. The waves detected for the longer time scans in the Fe^{II}(SAPH-2) system is similar to the hydroxy polymeric Fe^{II} species which are observed for $Fe(H_2O)_6^{2+}$ alone, adjusted to pH 8.23, in Fig. 6A. These waves are clearly different from mononuclear $Fe(H_2O)_6^{2+}$ at pH = 6.72 shown in Fig. 6B. Also, precipitation of green $Fe(OH)_2$ is in evidence in the bulk solution at pH = 8.23 (Fig. 6A) when no SAPH-2 is present.

The observation of loss in signal amplitude at pH = 6.94 (Fig. 5C) requires unwrapping of the coordination of SAPH-2 from the Fe^{III} complex, competitive with the rereduction on the cathodic sweep. The growth of the polymer in Fig. 6C at pH values greater than or equal to 7.71 can be explained by the formation of a dimeric iron complex with partial coordination of the SAPH-2 ligand (Scheme 4). The dimeric product, induced by oxidation at the glassy carbon electrode, exhibits two oxidation and two reduction waves (at *ca.* +0.10 and −0.34 V) which suggests retention of the core structure throughout the electrochemical changes of this species.

The results obtained for Fe^{II}(SAPH-2) by cyclic voltammetry are most important in regards to the

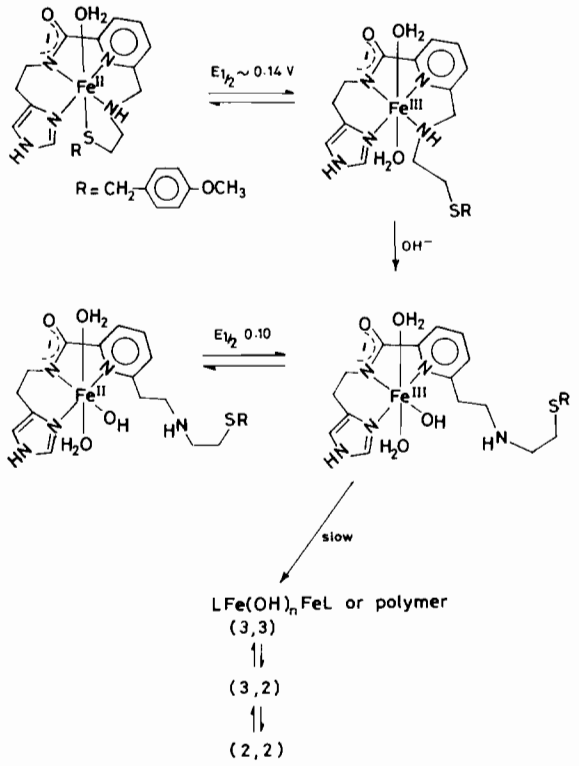

Scheme 4.

differing electrochemical behavior of Fe^{II}(SAPH-3). The free ligand SAPH-3 is easier to oxidize with increasing pH, but all waves are irreversible: pH 3.00 to 4.87, no wave; pH 6.96, $E_{1/2}$ ~0.89 V; pH 10.05, $E_{1/2}$ ~0.75 V. The free ligand cyclic voltammogram of SAPH-3 (pH = 6.96) is shown in Fig. 7A at 6.67×10^{-3} M, $\mu = 0.10$ $NaClO_4$, $T = 22$ °C. When Fe^{II} is added and the pH is adjusted upward to achieve coordination, the orange–pink form (pH = 5.70 to 5.90) shows a reversible wave (Fig. 7B-1) with $E_{1/2} = 0.22$ V in agreement with the differential pulse experiment. This species corresponds to **2B'** in Scheme 3. Upon increasing the pH to 6.90 which induces deprotonation of the amide moiety, forming species **2B**, a rapid scan within 45 s of pH adjustment reveals cyclic voltammogram 7B-2. A repetitive scan shows loss of this signal (scan 7B-3). The decay of the signal is not due to demetallation because restirring of the solution to replace the glassy carbon monolayer solution with the bulk, followed by scan 7B-4 shows the absence wave at *ca.* 0.14 V for species **2B**. These changes could be repeated by adjusting the solution pH below 5.90 followed by readjustment to pH 6.90. In this way the decay of the wave 7B-2 was shown to involve the sulfhydryl ring closure with $k = 9.6 \times 10^{-2}$ s^{-1}. This process converts species **2B** into **2C** in Scheme 3.

It is of importance to note that axial coordination of the sulfhydryl group of SAPH-3 produces an

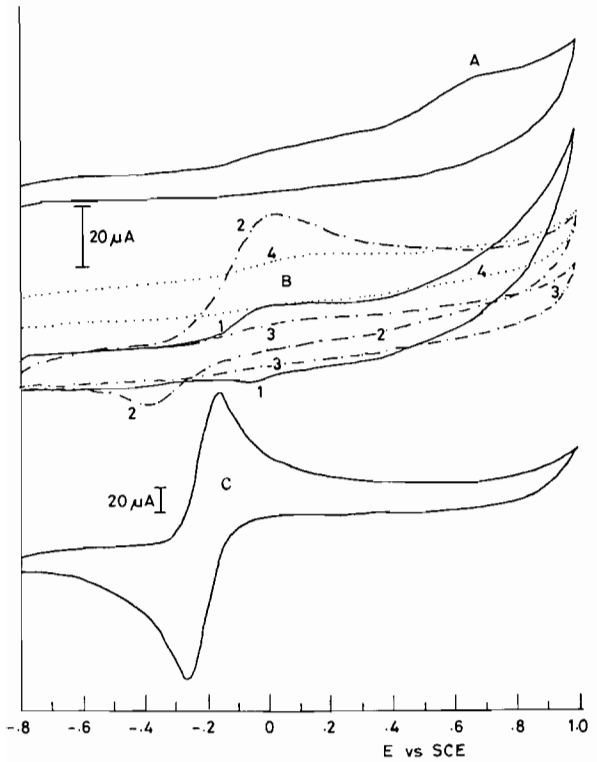

Fig. 7. Cyclic voltammograms of Fe^{II}(SAPH-3) system: (A) SAPH-3 ligand alone, pH = 6.96, (B) $[Fe^{II}(SAPH\text{-}3)]_i = 6.60 \times 10^{-3}$ M; curve 1, pH adjusted to 5.90 scanned twice; curve 2 pH adjusted to 6.90 and scanned at less than 45 s delay at 50 mV/s; curve 3, second scan at 50 mV/s of solution in curve 2; curve 4, bulk solution stirred and rescanned; curve 4 was displaced from curve 3 for visualization, but it is nearly the same. (C) Fe^{II}(SAPH-2) system at 6.60×10^{-3} M, pH = 4.95 with 6.60×10^{-3} M $[Ru(NH_3)_6]Cl_3$ added; current amplitude was suppressed 2.5× to record the reversible $Ru^{II/III}$ couple.

electrochemically inactive complex for Fe^{II}(SAPH-3) above pH 6.90. Therefore upon coordination of the sulfhydryl moiety no simple one electron oxidation process is obtained. This implies a strong mixing of orbitals from Fe^{II} and the axial sulfhydryl donor. Thus the axial Fe–S bond of Fe^{II}(SAPH-3) is much more covalent than the axial Fe–N (imidazole) bond of Fe^{II}(HAPH) which exhibits a reversible wave ($E_{1/2} = 0.092$ V) [25]. The absence of an electrochemical wave from –0.64 to +1.2 V *versus* NHE prompted a concern that adsorption of the complex or ligand on the glassy carbon surface could be the cause of the absence of a signal. This possible complication was ruled out by the addition of 6.60×10^{-3} M $Ru(NH_3)_6Cl_3$. The easily distinguished signal of the reversible $Ru(NH_3)_6^{3+/2+}$ couple in the presence of the Fe^{II}(SAPH-3) complex was obtained (Fig. 7C). $Ru(NH_3)_6^{3+}$ did not act as a chemical mediator for the Fe^{II}(SAPH-3) complex with the glassy carbon electrode; no other waves were observed. The Fe^{II}(SAPH-3) complex in form **2C** was shown to be chemically oxidizable by two electron oxidants. Either O_2 or Ru^{IV} rapidly oxidizes Fe^{II}(SAPH-3) with a subsequent (<60 s) demetallation to hydrated Fe_2O_3. The Ru^{IV} oxidant was produced by localized addition of concentrated NaOH. $Ru(NH_3)_6^{3+}$ is known to disproportionate into $Ru(NH_3)_6^{2+}$ and $Ru(NH_3)_6^{4+}$ under these conditions. A dark green oxidation product of Fe^{II}(SAPH-3) was seen in the high OH^- region near the syringe tip for addition of NaOH as when Fe^{II}(SAPH-3) is oxidized by O_2.

In the cases of Fe^{II}(HAPH) and Fe^{II}(BLM) the addition of CO produces the Fe^{II}(HAPH)CO and Fe^{II}(BLM)CO complexes. These have been shown to have electrochemical waves at 0.822 and 0.937 V, respectively [25]. The large positive shifts on coordination of CO is readily understood on the basis of the π-acceptor ability of the CO ligand stabilizing a low-spin Fe^{II} complex. Admission of CO for 25.0 min at 1.0 atm produced the anticipated yellow Fe^{II}(SAPH-3)CO complex [25, 29]. Again no detectable cyclic voltammetric waves were observed for the Fe^{II}(SAPH-3)CO complex. It may be inferred that the sulfhydryl donor is axially coordinated in the Fe^{II}(SAPH-3)CO complex because the Fe^{II}-(HAPH) and Fe^{II}(BLM) chromophores with axial N donors or H_2O yield reversible waves for their CO adducts. This requires an axial sulfhydryl chromophore to alter the electrochemical behavior.

Studies of the Fe^{III}(SAPH-series) Complexes

In the physiological pH range, the coordination of SAPH-1 and SAPH-3 to Fe(III) is anticipated to possess the imidazole, deprotonated amide, pyridine and amine donors as reported for Fe^{III}(BLM) and Fe^{III}(AMPHIS); this is further borne out by the spectral results which are described below. Sulfhydryl group binding was detected for Cu^{II}(SAPH-3) only in the pH range of about 3.5 to 5.5. An Fe(III) complex would be expected to participate in sulfhydryl coordination over a wider range due to the higher positive charge. Sulfhydryl coordination could occur even when the deprotonated amide is already present as a donor. The Fe^{III}(SAPH-1), complex was titrated spectrophotometrically as shown in Fig. 8A. Spectra were recorded rapidly to avoid turbidity due to the slow demetallation. A feature suggestive of an LMCT charge transfer band at $\lambda_{max} = 340$ nm, is observed at pH 3 where cationic Fe(III) complexes with coordinated H_2O are well-known to undergo hydrolysis. Using the reasonable assumption that imidazole, pyridine and possibly the amine donors of SAPH-1 are coordinated at pH 3, either an octahedral complex or trigonal bipyramidal species would possess three or two waters available for hydrolysis. The pH dependence and spectral changes that occur at *ca.* pH 5 to 6 are consistent with amide deprotonation as shown in the earlier section for Cu(II). Incorporation of this

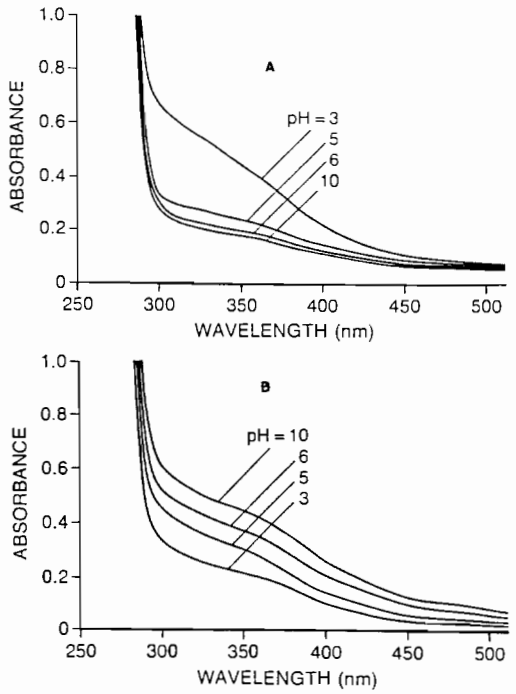

Fig. 8. UV–Vis spectra of 0.8 mM SAPH-1 or -3 containing an equimolar amount of $Fe(ClO_4)_3$ in aqueous solution. (A) SAPH-1 (–SMe) (B) SAPH-3 (–SH). pH was adjusted by addition of aqueous HCl or NaOH. Curves obtained at pH 7, 8 and 9 (not shown) were intermediate between pH 6 and 10.

strong ligand donor should shift the ligand field transitions to higher energy. The negative charge of the deprotonated amide will reverse the ability of Fe(III) to acidify coordinated water. Thus, the LMCT associated with charge transfer from OH^- to Fe(III) is lost with amide coordination. These spectral changes (Fig. 8A) infer the changes in coordination at Fe(III) shown for SAPH-1.

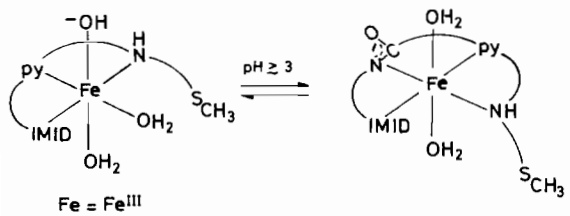

In contrast to Fe^{III}(SAPH-1), the Fe^{III}(SAPH-3) shows an increase in absorbance from pH 3 to pH 10 (Fig. 8B), and the initial intensity at 340 nm is less than for Fe^{III}(SAPH-1). The increase in absorbance throughout the pH range of 7 units is not accommodated by a single pH-dependent change such as amide coordination. SAPH-3 has three potentially ionizable groups: imidazole, amide and sulfhydryl. The pK_a of the imidazole functionability is above 10 for Fe^{III}(BLM) and Co^{III}(BLM) [30]. The pK_a of imidazole groups with cationic metal centers of +3 charge are all above 10 except for Ru(III) [31] and Cr(III) [32]. It is reasonable to conclude that imidazole formation is not responsible for any of the changes observed for Fe^{III}(SAPH-3). This is because the amide deprotonation step should occur near pH 5 or 6 as seen for the identical ligand except for the $S\text{-}CH_3$ blocking group in SAPH-1. Amide coordination will lower the ability of the Fe^{III}(SAPH-1) complex to ionize imidazole; thus the imidazole/imidazolate equilibrium will shift by at least 2 pK_a units above 10. Therefore, only the amide and sulfhydryl moieties need be considered as contributors to the changing ligand field implied by the spectrum in Fig. 8B.

Abbreviating the amide and sulfhydryl titratable groups of SAPH-3 as LHSH, one can write at least four contributing, overlapping equilibria that are suggested by Fig. 5B. Based on the ESR observations of

$$Fe^{III}(LHSH)^{3+} \overset{K_1}{\rightleftharpoons} Fe^{III}(LHS)^{2+} + H_3O^+ \quad (1)$$

$$Fe^{III}(LHSH)^{3+} \overset{K_2}{\rightleftharpoons} Fe^{III}(LSH)^{2+} + H_3O^+ \quad (2)$$

$$Fe^{III}(LHS)^{2+} \overset{K_3}{\rightleftharpoons} Fe^{III}(LS)^{+} + H_3O^+ \quad (3)$$

$$Fe^{III}(LSH)^{2+} \overset{K_4}{\rightleftharpoons} Fe^{III}(LS)^{+} + H_3O^+ \quad (4)$$

the Cu^{II}(SAPH-3) complex, an estimate of $K_1 = 10^{-3}$ M can be made. The related spectral results for Fe^{III}-(SAPH-1) allows K_2 to be estimated as 10^{-5} M. This is *ca.* 1.5 log units lower than for the Fe^{II} complex of HAPH and is consistent with the greater charge on Fe^{III}. Presence of an anionic sulfhydryl should reduce the ability of Fe(III) to assist amide deprotonation, thus, the value of K_3 should be between two and three orders of magnitude lower than K_2, e.g. $K_3 = 5 \times 10^{-8}$ M. Likewise, presence of an anionic coordinated amide should lower the ability of Fe(III) to assist deprotonation of the free sulfhydryl. The last equilibrium is probably close to the value to ionization of the free SAPH-3 ligand ($K_4 = 10^{-10}$ M). These overlapping equilibria provide a fraction of total Fe(III) as a complex with a bound sulfhydryl group, species $Fe(LHS)^{2+}$ and $Fe(LS)^+$, over the entire pH range because the equilibria pK_as of *ca.* 3.0, 5.0, 7.3, 10.0 are not sufficiently far apart that only one species is dominant. However, amide coordination or sulfhydryl coordination, present in all forms except $Fe(LHSH)^{3+}$, protects the complex against hydrolysis of coordinated H_2O and explains the absence of an LMCT transition as seen in the Fe^{III}(SAPH-1) case.

Additional evidence for the presence of coordinated sulfhydryl is given by the longer wavelength components, $\lambda > 400$ nm, which implicates an LMCT transition from a ligand more readily photooxidized

than OH^-. This is logically the RS^- chromophore of the deprotonated SAPH-3 ligand. The scheme below illustrates the coordination changes required to obtain a gradual increase in absorbance from 300 to 500 nm over pH range of 3 to 10.

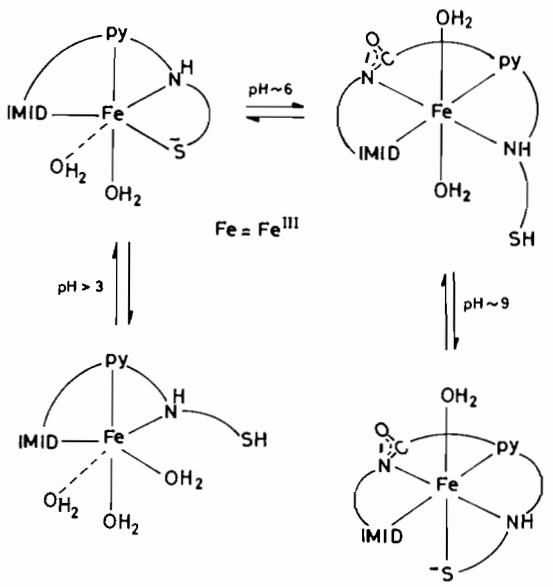

Spin Trapping Studies

Spin trapping studies were carried out using the well-known PBN and DMPO traps for HO·, HO_2·, O_2^-, and organic radicals derived from them in the presence of ethanol as a mediator. The technique has been reviewed by Janzen [33] and by Evans [34]. The experimental procedures and a discussion of the use of mediators has been presented in prior manuscripts [35–37]. The mechanism of attack on DNA strands by the Fe^{II}(BLM) system may involve a ferryl oxygen (Fe^{III}–O-atom) complex under conditions of low available Fe^{II} [4, 5a]. At higher concentrations (*ca.* 1.0×10^{-3} M *in vitro*) $Fe^{II}(BLM)/O_2$ generates copious amounts of HO_2· and HO· which are trapped by DMPO [29]. The ability of the synthesized Fe^{II}(SAPH1-3) and Fe^{II}(DAPHS4-6) complexes to activate O_2 at the higher *in vitro* concentrations was deemed a useful test of their oxygen radical generating activity in comparison with Fe^{II}(BLM) and Fe^{II}(AMPHIS). This method would not detect Fe^{III}–O atom intermediates which would be rapidly reduced by additional Fe^{II} at higher concentrations above the intercellular level.

The Fe^{II}(AMPHIS) complex was prepared under Ar in aqueous solution from weighed amounts of AMPHIS and $Fe(NH_4)_2(SO_4)_2 \cdot 6H_2O$. When O_2 was bubbled through a solution of *ca.* 1.0×10^{-3} M Fe^{II}(AMPHIS) in the presence of 1 M ethanol with PBN at *ca.* 1.0×10^{-2} M, a radical characteristic of [CH_3CHOH] was trapped; ($a_N = 16.4$ G, $a_H = 3.5$ G) [36, 37]. This confirms the report by Henichart *et al.* [8] that the Fe^{II}(AMPHIS) complex reacts with O_2 to produce HO·. The presence of ethanol acts as a scavenger for HO· to yield the trappable [CH_3CHOH]· species. When Fe^{II}(SAPH-1) was treated in an identical manner, the same radical adduct of PBN was trapped, but at one tenth of the signal amplitude produced by $Fe^{II}(AMPHIS)/O_2$ [38].

Attempts to trap radicals from the O_2 oxidation of Fe^{II}(SAPH-3) did not result in detectable radical signals after 30 s reaction and 30 additional seconds ESR tuning time for either PBN or DMPO radical traps at *ca.* 0.24 M. A free $Fe^{II}/DMPO/O_2$ blank yielded no radicals at these concentrations [37]. Identical conditions resulted in OH· being trapped with $Fe^{II}(BLM)/O_2$ or Fe^{II}(HAPH) with O_2 [29]. Since both of SAPH-3 and DAPHS-6 possess oxidizable sulfhydryl groups, it is possible that the –SH chromophore suffers a concerted $2e^-$ oxidation with the Fe^{II} center or attack by HO·, O_2^- or another oxygen-centered radical prior to the dissociation of the radical from the solvation cage of the Fe^{III}-(SAPH-3)O_2^- or Fe^{III}(DAPHS-6)O_2^- intermediate. This explanation is in keeping with observable reactivity for the Fe^{II}(SAPH-1) complex which carries a protected $-SCH_3$ moiety and the green intermediates observed visually during autoxidation of Fe^{II}(SAPH-3). It has been reported elsewhere that sulfhydryl containing compounds such as dithiothreitol (DTT) will successfully quench radicals produced by the autoxidation of $Fe^{II}(edta)^{2-}$ [36, 37]. The presence of the peroxo complex, $Fe^{III}(edta)(O_2H)^{2-}$, is in evidence from the product spectrum, thus the intermediate superoxo complex, $Fe^{II}(edta)O_2^-$, is rapidly reduced by DTT faster than it can form secondary radicals which are trapped by DMPO in the absence of DTT [37]. Therefore the presence of the terminal sulfhydryl group is ultimately detrimental to oxygen radical production by Fe^{II} complexes, either intramolecularly with Fe^{II}(SAPH-3) or intermolecularly with $Fe(edta)^{2-}$ and DTT.

When Fe^{II}(SAPH-3) was oxidized by H_2O_2 in the presence of DMPO, no radical adduct HODMPO· was observed. Copious amounts of HODMPO· ($a_N = a_H = 15.0$ G) were detected for the $Fe(edta)^{2-}/H_2O_2$/DMPO system on the same date of study and a comparable level of HO· is formed with Fe^{II}(HAPH) [29]. Therefore Fe^{II}(SAPH-3) produced no trappable radicals from either O_2 or H_2O_2 oxidation. Since the H_2O_2 one-electron reduction product must form HO·, the HO· species must be immediately reduced before it escapes the reaction cage. The only logical explanations are the attack of HO· on the sulfhydryl ligand or the transfer of two electrons together from the Fe^{II}-sulfhydryl chromophore. Thus Fe^{II}(SAPH-3) acts as essentially a 2-electron reagent toward either O_2 or H_2O_2. In addition, sulfhydryl coordination in Fe^{II}(SAPH-3) renders this complex chemically inert to a $1e^-$ oxidation at glassy carbon up to +1.24 V.

Conclusions

Substitution of the primary amino group by the thio function almost eliminates the ability to generate diffusable oxygen radicals in these simplified models of BLM. Visible spectra and electrochemical data indicate the sulfhydryl group is bound, depending on pH, to Fe(II) and Fe(III). The ESR data indicates that for the Cu(II) complexes of the SAPH and DAPHS series, there are significant departures from the octahedral structures proposed for PYML and AMPHIS outside the physiological pH range. Similar species of lower ligation are observed for Cu^{II}BLM by CD spectra [16]. The main factor in the impairment in the ability to mediate formation of diffusable oxygen radicals appears to be a direct $2e^-$ oxidation of the Fe^{II}–SR unit or that if free radicals are formed they are quickly extinguished by the nearby SH groups. The thiol function in SAPH-3 or DAPHS-6 is somewhat in a susceptible position for attack by free radicals, unlike the SH group of cytochrome P-450 where a massive organic layer covers the sulfhydryl moiety. Thus in an 'unprotected' molecule (e.g. SAPH-3 and DAPHS-6), the –SH group may undergo rapid oxidation. The identical unit, save for the replacement of SH by imidazole is quite active [29]. The –SH or $-S^-$ donor may also compete with water molecules for coordination of the central metal and the dissociated form may have a lower reactivity as observed for Fe^{II}(SAPH-1)/O_2. In either case, the ability to mediate active oxygen would suffer. Hydrophobic groups apparently are important in increasing the active oxygen ability of a number of recently synthesized analogs of PYML [38]. In fact, t-butyl esters of some substituted PYML analogs have shown active oxygenation capability approaching that of BLM [38b]. It should be noted that the $2e^-$ reduction of O_2 by Fe^{II}(SAPH-3) certainly parallels the $2e^-$ activation of O_2 by the P-450 enzyme.

Experimental

Melting points were determined on a Thomas-Hoover apparatus and are uncorrected. IR spectra were recorded with a Perkin-Elmer 267 Grating Infrared Spectrophotometer or a Digilab FTS 15/80. UV–Vis spectra were obtained with a Varian DMS 100 UV–Vis spectrophotometer or Varian-Cary 118C spectrophotometer. ^{1}H and ^{13}C NMR spectra were obtained with a Jeol FX90Q Fourier transform spectrometer operating at 89.55 and 22.50 MHz respectively, with TMS as a reference. High resolution mass spectral analysis were conducted on a V6 70-G double focusing mass spectrometer. Low resolution mass spectral analyses were conducted on a Finnigan 3200 mass spectrometer at 70 eV. Microanalyses were performed for synthesized compounds at Galbraith Laboratories, Inc., Knoxville, TN. Analytical thin-layer chromatography was conducted with Kodak silica gel precoated plastic chromatogram sheets impregnated with a fluorescent indicator. Preparative thin-layer chromatography was performed on Analtech silica gel GF (1000 microns in thickness). Column chromatography utilized Mallinckrodt analytical grade silicic acid powder.

Methyl 6-[[[2-(methylthio)ethyl]amino]methyl]-2-pyridinecarboxylate (8)

To a solution of *S*-methylcysteamine (260 mg, 2.9 mmol) in methanol (10 ml) was added two drops of the indicator dye bromocresol purple (1% in methanol). The pH was adjusted to 6 with the addition of 5 M HCl in methanol, as indicated by a yellow–green color. Size 3A molecular sieves were then added to the flask. The solution was then combined with a solution of the aldehyde **7** (430 mg, 2.6 mmol) in methanol (10 ml). This mixture was stirred for 1.5 h at which time sodium cyanoborohydride (130 mg, 2.0 mmol) was added. The solution was then stirred for an additional 15 h. Afterwards, saturated $NaHCO_3$ solution (10 ml) was added to the reaction mixture. The basic solution was then extracted with $CHCl_3$ (3 × 20 ml). The organic fractions were combined and dried over $MgSO_4$. Subsequent evaporation of solvent yielded a green oil. The oil was purified by preparative TLC (MeOH–CH_2Cl_2 = 7.5:100) to yield the product **8** (440 mg, 70% yield): ^{1}H NMR ($CDCl_3$) δ 8.1–7.4 (m, 3H, PyrH), 4.07 (s, 2H, PyrCH_2N), 4.00 (s, 3H, $COOCH_3$), 3.0–2.5 (m, 4H, SCH_2CH_2N), 2.10 (s, 3H, SCH_3); ^{13}C NMR ($CDCl_3$) δ 165.8 (*C*$OOCH_3$), 160.6 (PyrC_2), 147.6 (PyrC_6), 137.4 (PyrC_4), 125.6 (PyrC_3), 123.6 (PyrC_5), 58.4 (Pyr*C*H_2N), 52.8 (COO*C*H_3), 47.7 (SCH_2CH_2N), 34.5 (S*C*H_2CH_2N), 15.3 (SCH_3); IR ($CHCl_3$) ν cm^{-1} 3390 (br, N–H), 1718 (ester C=O); MS *m/z*, 240 (M^+), 193, 179 (100%), 165, 151.

Methyl 6-[[[2-[[(4-methoxyphenyl)methyl]thio]-ethyl]amino]methyl]-2-pyridinecarboxylate (9)

Analogous to the procedure described above for **8**, compound **9** was prepared from the aldehyde **7** (0.98 g, 4.97 mmol), *S*-(4-methoxybenzyl)cysteamine (820 mg, 4.97 mmol) and soldium cyanoborohydride (250 mg, 4.0 mmol) in a total volume of 25 ml of methanol. After workup the blue oil was purified by column chromatography (silicic acid, MeOH–CH_2Cl_2 = 2:98) to yield the desired product **9** (1.12 g, 65% yield): ^{1}H NMR ($CDCl_3$) δ 8.1–7.3 (m, 3H, PyrH), 7.0 (dd, 4H, Ar*H*), 3.98 (s, 5H, $COOCH_3$ and PyrCH_2N) 3.80 (s, 3H, ArOCH_3), 3.67 (s, 2H, SCH_2-Ar), 2.9–2.4 (m, 4H, SCH_2CH_2N), 2.4–2.1 (br s, 1H, NH); ^{13}C NMR ($CDCl_3$) δ 165.8 (ester C=O), 160.6 (PyrC_2), 158.7 (ArC_4), 147.6 (PyrC_6), 137.4 (PyrC_4), 130.3 (ArC_1), 129.9 (ArC_3 and C_5), 125.5 (PyrC_3), 123.5 (PyrC_5), 114.0 (ArC_2 and C_6), 55.3 (ArOCH_3),

54.7 (PyrCH_2NH), 52.8 ($COOCH_3$), 48.1 (SCH_2CH_2-N), 35.6 (SCH_2Ar), 31.6 (SCH_2CH_2N); IR ($CHCl_3$) ν cm^{-1} 3400–3200 (N–H), 1718 (ester C=O); MS, *m/z* 346 (M^+), 225, 193, 179 (100%); HRMS, *m/z* 346.1321 ($C_{18}H_{22}N_2O_3S$ requires 346.1351).

A hydrobromide was made by passing HBr gas into a MeOH–Et_2O solution of **9**. The resulting solid was filtered, washed with ether, then acetone, and dried: melting point (m.p.) 114–115 °C; ^{1}H NMR (D_2O), δ 8.2–7.9 (m, 2H, PyrH), 7.6 (dd, 1H, PyrH), 7.0 (dd, 4 H, ArH), 4.34 (s, 2H, PyrCH_2N), 3.98 (s, 3H, $COOCH_3$), 3.73 (s, 3H, ArOCH_3), 3.68 (s, 2H, SCH_2Ar), 3.2–2.9 (m, 2H, SCH_2CH_2N), 2.9–2.6 (m, 2H, SCH_2CH_2N).

N-[2-(1H-Imidazol-4-yl)ethyl]-6-[[[2-(methylthio)-ethyl]amino]methyl]-2-pyridinecarboxamide (SAPH-1)

The ester **8** (700 mg, 2.9 mmol) was dissolved in 10 ml of MeOH and treated with an excess of histamine (1.2 g, 10.4 mmol). The reaction was stirred at room temperature for eight days. The methanol was then evaporated from the solution to give a green oil which was purified by preparative TLC [silica gel GF, CH_3NH_2 (40% aq soln)–MeOH–$CHCl_3$ = 10:10:80]. The pure product was recovered as a brown oil (550 mg, 59% yield): ^{1}H NMR ($CDCl_3$) δ 8.7–8.2 (br t, 1H, CONHCH$_2$), 8.1–7.1 (m, 4H, PyrH and ImidC_5H), 6.85 (s, 1H, ImidC_2H), 3.97 (s, 2H, PyrCH_2N), 3.9–3.5 (m, 2H, $CONHCH_2$), 3.1–2.4 (m, 6H, SCH_2CH_2N and ImidCH_2), 2.08 (s, 3H, SCH_3); ^{13}C NMR ($CDCl_3$) δ 164.5 (CONH), 158.2 (PyrC_2), 149.4 (PyrC_6), 137.8 (PyrC_4), 135.2 (ImidC_4), 134.9 (ImidC_2), 124.7 (ImidC_5), 120.4 (PyrC_3), 116.7 (PyrC_5), 53.9 (PyrCH_2N), 47.4 (SCH_2CH_2N), 39.4 ($CONHCH_2$), 34.4 (SCH_2CH_2N), 27.2 (ImidCH_2), 15.3 (SCH_3); IR ($CHCl_3$) ν cm^{-1} 3250 (broad, N–H), 1660 (amide C=O); HRMS, *m/z* 319.1487 ($C_{15}H_{21}N_5OS$ requires 319.1484).

The bis dihydrogen oxalate of **1** was made and recrystallized from aqueous methanol: m.p. 194–195 °C; ^{1}H NMR (D_2O) δ 8.55 (d, 1H, ImidC_2H), 8.1–7.8 (m, 2H, PyrC_3- and C_5H), 7.7–7.5 (m, 1H, PyrC_4H), 7.25 (s, 1H, ImidC_5H), 4.50 (s, 2H, PyrCH_2N), 3.8–3.7 (m, 2H, $CONHCH_2CH_2$), 3.40 (t, 2H, ImidCH_2-CH_2), 3.55 (t, 2H, SCH_2CH_2N), 3.4–3.1 (t, 2H, SCH_2CH_2N), 2.05 (s, 3H, SCH_3); *Anal.* Calc. for $C_{19}H_{25}N_5O_9S$: C, 45.69; H, 5.04; N, 14.02; S, 6.42. Found: C, 46.13; H, 5.15; N, 14.50; S, 6.76%.

N-[2-(1H-Imidazol-4-yl)ethyl]-6-[[[2-[[(4-methoxyphenyl)methyl]thio]ethyl]amino]methyl]-2-pyridinecarboxamide (SAPH-2)

Similar to the procedure for the preparation of **1**, the ester **9** (900 mg, 2.6 mmol) was dissolved in methanol (10 ml). To this solution a four molar excess of histamine (1.2 g, 10.4 mmol) was added. The reaction was stirred at room temperature for six days. The methanol was then evaporated from the solution to give a brown oil. The oil was dissolved in chloroform and washed with H_2O (4 × 10 ml), to facilitate the removal of excess histamine. The chloroform layer was dried over $MgSO_4$ and evaporated. The resulting oil was purified by column chromatography (silicic acid, MeOH–CH_2Cl_2 = 10:100). Alternatively, small quantities were purified by preparative TLC [silica gel GF, CH_3NH_2 (40% aq soln)–MeOH–$CHCl_3$ = 5:7:140]. The pure product was recovered as a brown oil (660 mg, 60% yield): ^{1}H NMR ($CDCl_3$) δ 8.8–8.3 (br t, 1H, CONHCH$_2$), 8.2–7.3 (m, 4H, PyrH and ImidC_5H), 7.3–6.6 (m, 5H, ArH and ImidC_2H), 3.93 (s, 2H, PyrCH_2N) 3.80 (s, 3H, ArOCH_3) 3.65 (s, 2H, SCH_2Ar), 3.8–3.6 (m, 2H, $CONHCH_2$), 3.1–2.4 (m, 6H, SCH_2CH_2N and ImidCH_2); ^{13}C NMR ($CDCl_3$) δ 164.5(CONH), 158.6 (PyrC_2), 158.4 (ArC_4), 149.3 (PyrC_6), 137.7 (PyrC_4), 135.2 (ImidC_4), 134.9 (ImidC_2), 130.1 (ArC_1) 129.8 (ArC_3 and C_5) 124.6 (ImidC_5), 120.3 (PyrC_3), 116.7 (PyrC_5), 113.9 (ArC_2 and C_6), 55.2 (ArOCH_3), 54.0 (PyrCH_2N), 47.8 (SCH_2CH_2N), 39.2 ($CONHCH_2$), 35.6 (SCH_2Ar), 31.6 (SCH_2CH_2N), 27.2 (ImidCH_2); IR ($CHCl_3$) ν cm^{-1} 3400–3200 (b, N–H), 1650 (amide C=O); MS, *m/z* 426 ($M+1^+$), 425 (M^+), 304, 272, 258 (100%).

A dihydrogen oxalate of **2** was prepared and recrystallized from aqueous methanol: m.p. 183–184 °C; ^{1}H NMR (D_2O) δ 8.55 (d, 1H, ImidC_2H), 8.2–8.0 (m, 2H, PyrC_3- and C_5H), 7.65 (t, 1H, PyrC_4H), 7.16 (s, 1H, ImidC_5H), 7.2–6.7 (dd, 4H, ArH), 4.35 (s, 2H, PyrCH_2N), 3.75 (s, 3H, ArOCH_3), 3.8–3.6 (m, 2H, $CONHCH_2$), 3.65 (s, 2H, SCH_2Ar), 3.2–2.7 (m, 6H, ImidCH_2 and $SCH_2CH_2NH_2$). *Anal.* Calc. for $C_{26}H_{31}N_5O_{10}S$: C, 51.56; H, 5.16; N, 11.57; S, 5.30. Found: C, 51.97; H, 5.23; N, 11.53; S, 5.66%.

N-[2-(1H-Imidazol-4-yl)ethyl]-6-[[(2-mercaptoethyl)-amino]methyl]-2-pyridinecarboxamide trihydrochloride (SAPH-3)

Method A [12]

In a teflon reaction chamber the S-protected amine **2** (650 mg, 1.53 mmol) was combined with anisole (660 mg, 6.12 mmol). Liquid HF (5 ml) was then condensed into a preliminary teflon vessel which contained CoF_3 (0.5 g) as a drying agent. The HF was then distilled into the reaction chamber. The mixture was stirred for 0.5 h at 0 °C. Afterwards, the HF was removed with a water aspirator and the reaction container was placed under high vacuum (0.6 mmHg) for a 12 h period. Subsequently, the oil remaining in the reaction chamber was dissolved in CH_2Cl_2 (5 ml) and extracted with 1 N HCl (3 × 5 ml). The aqueous fractions were combined and lyophilized. A hygroscopic solid found to be the trihydrochloride of **2** was recovered (510 mg, 80% yield): ^{1}H NMR (D_2O) δ 9.02 (s, 1H, ImidC_2H), 8.6–8.2 (m, 2H, PyrC_3- and

C_5H), 8.2–7.9 (m, 1H, PyrC$_4H$), 7.70 (s, 1H, ImidC$_5$-H), 4.98 (s, 2H, PyrCH_2N), 4.2 (m, 2H, CONHCH_2-CH_2), 3.84 (t, 2H, ImidCH_2CH_2), 3.6–3.1 (m, 4H, SCH_2CH_2N); ^{13}C NMR (D_2O) δ 167.0 (CONH) 151.3, 149.5 (PyrC$_2$ and C$_6$), 140,9 (PyrC$_4$), 134.4, 132.0 (PyrC$_3$ and C$_5$), 127.4 (ImidC$_2$), 123.3 (ImidC$_4$), 117.4 (ImidC$_5$), 51.2, 50.9 (PyrC$H_2NH_2^+$-CH_2), 39.4 (CONHCH_2), 25.4 (ImidCH_2), 21.2 (SCH_2CH_2N); IR (KBr) ν cm^{-1} 3425 (N–H), 1640 (amide C=O); MS *m/z*, 305 (*M*$^+$), 272 (100%), 258, 245.

Method B

The S-protected amine **2** (590 mg, 1.4 mmol) was dissolved in trifluoroacetic acid (10 ml). Anisole (600 mg, 5.6 mmol) was then added to the reaction flask. The mixture was heated under condenser and drying tube for 1 h at 90 °C. Subsequently the acid was removed under water aspirator and a brown oil remained in the flask. The oil was dissolved in CH_2Cl_2 (5 ml) and extracted with 1 N HCl (3 × 5 ml). The aqueous fractions were combined and freeze-dried to yield a hygroscopic solid found to be the trihydrochloride (490 mg, 85% yield). The spectral data was identical to that of method A. The free base of **3** was prepared by placing the hydrochloride over a Bio-Rad AG 50 W-X8 analytical grade cation exchange resin. Elution with H_2O was followed by 1% aqueous ammonia while bubbling argon gas through the eluates. Lyophilization of collected fractions produced a 90% recovery of the free base of **3**: ^{1}H NMR ($CDCl_3$) δ 8.8–8.3 (br t, 1H, CONHCH$_2$), 8.2–7.0 (m, 4H, three PyrH and ImidC$_2$H), 6.83 (s, 1H, ImidC$_5$H), 3.93 (s, 2H, PyrCH_2N), 3.8–3.3 (m, 2H, ImidCH_2-CH_2), 3.1–2.3 (m, 6H, SCH_2CH_2N and CONHCH_2); HRMS, *m/z* 305.1313 ($C_{14}H_{19}N_5OS$ requires 305.1317).

Treatment of **3** with $ZnCl_2$ gave a precipitate which was recrystallized from methanol to yield white crystals: m.p. 212–214 °C; NMR data was identical to that for the trihydrochloride of **3**. *Anal.* Calc. for $C_{14}H_{22}Cl_3N_5OS \cdot 0.75ZnCl_2 \cdot 0.75H_2O$: C, 31.57; H, 4.46; N, 13.15; S, 6.02; Zn, 9.21. Found: C, 31.49; H, 4.42; N, 12.96; S, 6.33; Zn, 8.94%.

Methyl 6-[[[2-(methylthio)ethyl]amino]carbonyl-2-pyridinecarboxylate (11)

To a solution of the acid ester **10**, (1.81 g, 0.01 mol) in 25 ml of dioxane was added a solution of HOBT (2.29 g, 0.015 mol) in 25 ml of dioxane followed by a solution of DCC (2.06 g, 0.01 mol) in 20 ml of CH_2Cl_2. After stirring for 1 h at 0–5 °C, the precipitate was filtered and washed several times with CH_2Cl_2. The filtrate was then evaporated to *ca.* 50 ml, and *S*-methyl cysteamine (0.91 g, 0.01 ml) added. The reaction mixture was then stirred overnight at room temperature, filtered to remove solid, washed with 10% aq $NaHCO_3$ (2 × 15 ml), H_2O (1 × 15 ml), and finally dried (Na_2SO_4). Removal of solvent *in vacuo* produced 2.29 g of a reddish-brown oil. TLC revealed predominantly product but small amounts of impurities were also detected. Further purification was achieved by chromatography on a 4 cm × 66 cm column containing 225 g of silicic acid. Elution with CH_2Cl_2–MeOH = 99:1 gave 1.16 g (46%) of product sufficiently pure for ensuing reactions. An analytical sample was prepared by collection of samples eluted from an HPLC column (C-18 reverse phase; CH_3CN–H_2O = 20:80) and evaporation of solvent to give **11** as a yellow oil. ^{1}H NMR ($CDCl_3$) δ 8.6–8.4 (br s, 1H, CONH), 8.4–7.8 (m, 3H, PyrH), 3.98 (s, 3H, $COOCH_3$), 3.65 (dd, 2H, CONHCH_2CH_2), 2.78 (t, 2H, SCH_2CH_2N), 2.16 (s, 3H, SCH_3). ^{13}C NMR ($CDCl_3$) δ 164.7 (ester C=O), 163.4 (amide C=O), 150.1 and 146.7 (PyrC$_2$ and PyrC$_6$), 138.5 (PyrC$_4$), 127.2 and 125.3 (PyrC$_3$ and C$_5$), 52.7 (COOCH_3), 38.6 (CONHCH_2), 33.7 (SCH_2CH_2N), 15.3 (SCH_3); IR (CS_2) ν cm^{-1} 3480 and 3375 (N–H), 1730 (ester C=O), 1680 (amide C=O); MS, *m/z* 254 (*M*$^+$), 239, 223, 207, 193, 181, 164, 136. *Anal.* Calc. for $C_{11}H_{14}N_2O_3S \cdot 0.75H_2O$: C, 49.32; H, 5.83; N, 10.46; S, 11.97. Found: C, 49.50; H, 5.92; N, 10.23; S, 12.06%.

Methyl 6-[[[2-[[(4-methoxyphenyl)methyl]thio]-ethyl]amino]carbonyl]-2-pyridinecarboxylate (12)

A mixture of 905 mg (5 mmol) of **10** and HOBT·H_2O (765 mg, 5 mmol) was dissolved in 5 ml of DMF and then cooled to 0 °C. A solution of DCC (1.030 g, 5 mmol) in 1 ml of DMF was then added and the entire mixture stirred for 1/2 h at 0 °C. During this time, a white solid appeared. A solution of *S*-(4-methoxybenzyl)cysteamine (985 mg, 5 mmol) in 1 ml of DMF was added and the temperature maintained for an additional 0.5 h. The mixture was then allowed to warm to room temperature and stirred an additional 5 h. Solvent was removed at high vacuum (35 °C) and the residue taken up in 25 ml of CH_2Cl_2. The organic portion was washed with 10% aq. citric acid (4 × 10 ml), water (1 × 10 ml) and finally with a saturated NaCl solution (1 × 10 ml). After drying ($MgSO_4$) and removal of the solvent, 1.80 g of an orange oil was obtained. TLC revealed three spots, but the major spot was the desired product. Further purification was achieved by chromatography on a 4 × 66 cm column containing silicic acid. Elution with 2% MeOH/CH_2Cl_2 gave 1.01 g of the product as a yellow oil and 0.60 g of additional material containing small amounts of impurities. Further workup of this latter fraction produced a sufficiently pure material which was combined with the yellow oil to give 1.56 g (86%) of **12**. ^{1}H NMR ($CDCl_3$) δ 8.6–7.8 (m, 3H, PyrH), 7.3–6.6 (m, 4H, ArH), 4.00 (s, 3H, $COOCH_3$), 3.75 (s, 3H, ArOCH_3), 3.70 (s, 2H, SCH_2Ar), 3.6–3.4 (m, 2H, CONHCH_2CH_2), 2.64 (t, 2H, SCH_2CH_2N); ^{13}C NMR ($CDCl_3$) δ 164.9 (ester

C=O), 163.4 (amide C=O), 158.7 (ArC_4), 146.6 ($PyrC_2$ and C_6), 138.4 ($PyrC_4$), 130.1 (ArC_1), 129.9 (ArC_3 and C_5), 127.1 and 125.3 ($PyrC_3$ and C_5), 113.9 (ArC_2 and C_6), 55.2 ($ArOCH_3$), 52.8 ($COOCH_3$), 38.8 (SCH_2Ar), 35.5 ($CONHCH_2$), 30.8 (SCH_2CH_2N); IR ($CHCl_3$) ν cm^{-1} 3390 (N–H), 1728 (ester C=O), 1670 (amide C=O); MS, *m/z* 360 (M^+), 239, 164, 136, 121 (100%).

N-[2-1H-Imidazol-4-yl)ethyl]-N'-[2-(methylthio)-ethyl] 2,6-pyridine-dicarboxamide (DAPHS-4)

In a stoppered flask, the ester **11** (508 mg, 2.0 mmol) was treated with a solution of histamine (1.0 g, 10 mmol) in 10 ml of methanol. The mixture was stirred at room temperature for 5 days after which time TLC analysis indicated all of the starting material had reacted. Upon removal of the solvent *in vacuo,* the oil was taken up in 5 ml of $CHCl_3$, which then was washed with water (3 X 3 ml) to remove the excess histamine, and finally with saturated NaCl (1 X 3 ml). After drying ($MgSO_4$) and evaporation of the solvent, 500 mg of **4** (75% yield) was obtained. An analytical sample was prepared by crystallization from CH_3CN to given an egg-white solid, m.p. 147.5–149 °C. ^1H NMR ($CDCl_3$) δ 9.4–9.1 · (br t, 1H, $CONHCH_2$), 8.9–8.6 (br t, 1H, $CONHCH_2$), 8.4–7.9 (m, 3H, PyrH) 7.62 (s, 1H, $ImidC_2H$) 6.87 (s, 1H, $ImidC_5H$), 3.9–3.5 (m, 4H two $CONHCH_2CH_2$), 3.1–2.6 (m, 4H, $ImidCH_2CH_2$ and SCH_2CH_2), 2.15 (s, 3H, SCH_3). ^{13}C NMR ($CDCl_3$) δ 164.0 (ester and amide C=O), 148.9 and 148.7 ($PyrC_2$ and $PyrC_6$), 139.0 ($PyrC_4$), 136.1 and 135.0 ($ImidC_2$ and C_4), 124.6 ($ImidC_5$), 116.3 (Pyr C_3 and C_5), 39.8 and 38.9 (both $CONHCH_2CH_2$), 33.6 (CH_2S), 26.8 ($ImidCH_2$), 15.3 (SCH_3). IR ($CHCl_3$) ν cm^{-1} 3290 (N–H), 1665 (amide C=O); MS, *m/z* 333 (M^+), 318, 286 (100%), 272, 252, 223. *Anal.* Calc. for $C_{15}H_{19}N_5O_2S$: C, 54.03; H, 5.74; N, 21.01; S, 9.62. Found: C, 54.16; H, 5.99; N, 20.69; S, 9.74%.

N-[2-(1H-Imidazol-4-yl)ethyl]-N'-[2-]](4-methoxy-phenyl)methyl]thiol]ethyl]2,6-pyridinecarboxamide hydrobromide (DAPHS-5)

Using the procedure described above for the amidation of **11**, the ester **12** (1.01 g, 2.8 mmol) and histamine (1.24 g, 11 mmol) in 6 ml of MeOH were stirred for three days. The product **5** (1.11 g, 90%) was obtained as an oil. A hydrobromide salt of the diamide was prepared by treating a portion of the oil with 10% aq HBr and setting the mixture in the refrigerator overnight. Recrystallization of the egg-white solid from acetonitrile (containing a small amount of MeOH) and drying (P_2O_5) under high vacuum at 45 °C gave **5**·HBr, m.p. 181–183 °C. ^1H NMR (CD_3OD) δ 8.78 (s, 1H, $ImidC_2H$), 8.4–8.2 (m, 3H, PyrH), 7.38 (s, 1H, $ImidC_5H$), 7.04 (dd, 4H, ArH), 3.11 (t, 2H, $ImidCH_2CH_2$) 2.70 (t, 2H, SCH_2CH_2N). IR (KBr) ν cm^{-1} 3450, 3320, 3280, 3100, and 2870 (N–H), 1680 and 1655 (amide C=O). *Anal.* Calc. for $C_{22}H_{26}BrN_5O_3S$: C, 50.77; H, 5.04; N, 13.46; S, 6.16. Found: C, 50.36; H, 5.28; N, 13.76; S, 6.39%.

N-[2(1H-Imidazol-4-yl)ethyl]-N'-(2-mercaptoethyl)-2,6-pyridinedicarboxamide (DAPHS-6)

To a 10 ml reaction-vial was added the diamide **5** (44 mg, 0.1 mmol), anisole (54 mg, 0.5 mmol) and trifluoroacetic acid (1.0 ml). The vessel was stoppered and heated to 90–95 °C for 1 h, after which time the mixture was cooled and evacuated at the water aspirator (40 °C). Nitrogen gas was introduced into the vacuum line and was also bubbled into solutions during the ensuing workup. The residue after evaporation was taken up in distilled water (2–3 ml) and washed with CH_2Cl_2 (3 X 1 ml). The aqueous solution was lyophilized to give 44 mg (quantitative yield) of **6** as the trifluoroacetate, containing no detectable impurities. ^1H NMR (CD_3OD) δ 8.79 (d, 1H, $ImidC_2H$), 8.4–8.0 (m, 3H, PyrH), 7.36 (d, 1H, $ImidC_5H$), 3.9–3.4 (m, 4H, two $CONHCH_2$), 3.10 (t, 2H, $ImidCH_2CH_2$), 2.75 (t, 2H, SCH_2CH_2N); IR (KBr) ν cm^{-1} 3700–3200 (N–H and OH), 1674 (C=O); MS, *m/z* 319 (M^+), 301, 286, 272, 238, 191, 181, 163; HRMS, *m/z* 319.1104 ($C_{14}H_{17}N_5O_2S$ requires 319.1103). The free base of **6** could be obtained as an oil, or other acid salts as glasses could be made after passing the trifluoroacetate over a cation exchange resin and eluting with the appropriate reagents. Both the free base and the salt forms gave positive Ellman's tests indicative of a sulfhydryl group.

ESR Spectra

Spectra of Cu(II) complexes were recorded at 113 K with a Varian E-4 EPR spectrometer at 20 mW power and 1.25 G modulation amplitude, tuned in the 9.07 GHz region. The details of sample preparation and operation have been given elsewhere [20].

Electrochemical Studies

Electrochemical measurements were performed using standard techniques on an IBM 225 Voltammetric Analyzer [25].

Spin-trapping Studies

N-Tert-butyl-α-phenylnitrone (PBN) and 5,5-dimethyl-1-pyrroline-*N*-oxide (DMPO) were obtained from Aldrich. All manipulations of Fe(II) complexes were performed by weighing samples of $Fe(NH_4)_2(SO_4)_2 \cdot 6H_2O$ such that an excess of chelating ligand (*ca.* 20%) was available in the final solution to assure no free $Fe(H_2O)_6^{2+}$ was present. Spin trapping procedures were the same as those of Myser and Shepherd [35, 37]; these references should be consulted for procedural details and other pertinent aspects of the spin trapping experiments of this report.

Acknowledgements

This research was supported in part by an institutional grant IN 58-W from the American Cancer Society to the University of Pittsburgh and also from the Central Research and Development Fund (University of Pittsburgh). Support for S. Siddiqui and R. E. Shepherd under National Science Foundation grant CHE-8417751 is gratefully acknowledged. Appreciation is also extended to Kathy Shander, David Parker and Monica Truesdell who assisted in some of the synthetic work and to Michael G. Elliott who conducted the differential pulse voltammetry experiments. Additionally, we thank Dr Michal Mokotoff for his aid in discussion of the synthetic schemes. AMPHIS was a gift supplied by Professor Henichart.

Results

1 (a) H. Umezawa, *Lloydia, 40* (1977) 67; (b) T. Takita, Y. Muraoka, T. Nakatani, A. Fujii, Y. Umezawa, H. Naganawa and H. J. Umezawa, *Antibiotics, 31* (1978) 801.
2 (a) M. Takeshita and A. P. Grollman, in S. M. Hecht (ed.), *Bleomycin, Chemical, Biochemical and Aspects,* Springer, New York, 1979, p. 207; (b) H. Kasai, H. Naganawa, T. Takita and H. J. Umezawa, *Antibiotics, 31* (1978) 1316; (c) H. Umezawa, *Prog. Biochem. Pharmacol., 11* (1976) 18; (d) Y. Sugiura and T. J. Kikuchi, *Antibiotics, 31* (1978) 1310.
3 (a) S. K. Carter, *Bleomycin Chemotherapy,* Academic Press, Orlando, FL, 1985, pp. 3–4; (b) R. A. Newman, M. R. Hacker and T. T. Sakai, *Toxicol. Appl. Pharmacol., 70* (1983) 373; (c) E. Ginsburg, T. E. Gram and M. A. Trush, *Cancer Chemother. Pharmacol., 12* (1984) 111.
4 S. M. Hecht, *Acc. Chem. Res., 19* (1986) 383.
5 (a) R. M. Burger, J. Peisach and S. B. Horowitz, *J. Biol. Chem., 256* (1981) 11636; (b) W. J. Caspary, C. Niziak, D. A. Lanzo, R. Friedman and N. R. Bachur, *Mol. Pharmacol., 16* (1979) 256; (c) J. W. Lown and S. K. Sim, *Biochem. Biophys. Res. Commun., 73* (1977) 814.
6 G. Padbury and S. Sligar, *J. Biol. Chem., 260* (1985) 7820.
7 Y. Sugiura, T. Suzuki, M. Otsuka, S. Kobayashi, M. Ohno, T. Takita and H. J. Umezawa, *J. Biol. Chem., 258* (1983) 1328.
8 (a) J.-P. Henichart, R. Houssin, J.-L. Bernier and J.-P. Catteau, *J. Chem. Soc., Chem. Commun.,* 1295 (1982); (b) J.-P. Henichart, J.-L. Bernier, R. Houssin, M. Lohez, A. Kenani and J.-P. Cattcau, *Biochem. Biophys. Res. Commun., 126* (1985) 1036.
9 S. J. Brown, P. K. Mascharak and D. W. Stephan, *J. Am. Chem. Soc., 110* (1988) 1996.
10 N. J. Oppenheimer, L. O. Rodriguez and S. M. Hecht, *Biochemistry, 19* (1980) 4096.
11 R. F. Borch, M. D. Bernstein and H. D. Durst, *J. Am. Chem. Soc., 93* (1971) 2897.
12 C. De Marco and D. Bognolo, *Arch. Biochem. Biophys., 98* (1962) 526.
13 (a) S. Sakakibara and Y. Shimonishi, *Bull. Chem. Soc. Jpn., 38* (1965) 1412; (b) S. Akabori, S. Sakakibara, Y. Shimonishi and Y. Nobuhara, *Bull. Chem. Soc. Jpn., 37* (1964) 433.
14 B. McCloskey, T. Lomis and J. F. Siuda, *Eighth Annual Pharmacy Undergraduate Research Seminar,* West Virginia University, November 12, 1986.
15 Y. Sugiura, T. Takita and H. Umezawa, Bleomycin antibiotics: metal complexes and their biological action, in H. Sigel (ed.), *Metal Ions in Biological Systems',* Vol. 19, Marcel Dekker, New York, 1985, pp. 81–108.
16 J.-P. Albertini and A. G. Garnier-Suillerot, *J. Inorg. Biochem., 25* (1985) 15.
17 (a) D. W. Margerum and G. R. Dukes, *Metal Ions in Biological Systems,* Vol. 1, Marcel Dekker, New York, 1974, pp. 157–212; (b) M. P. Youngblood, K. L. Chelleppa, C. E. Bannister and D. W. Margerum, *Inorg. Chem., 20* (1981) 1742.
18 (a) J. Mandel, *Ph.D. Thesis,* University of Pittsburgh, 1987; (b) J. Mandel and B. E. Douglas, *Inorg. Chim. Acta, 155* (1988) 55.
19 (a) B. J. Hathaway and D. E. Billing, *Coord. Chem. Rev., 5* (1970) 143; (b) J. Gazo, I. B. Bersuker, J. Garoj, M. Kabesova, J. Kohout, H. Langbelderova, M. Melnik, M. Serator and F. Valach, *Coord. Chem. Rev., 19* (1976) 253.
20 S. Siddiqui and R. E. Shepherd, *Inorg. Chem., 25* (1986) 3869.
21 (a) D. Kivelson and R. Nieman, *J. Chem. Phys., 35* (1961) 157; (b) H. R. Gersmann and J. D. Swalen, *J. Chem. Phys., 36* (1962) 3221; (c) A. K. Wiersema and J. J. Windle, *J. Chem. Phys., 68* (1964) 2316; (d) R. P. Bonomo and F. Riggi, *Chem. Phys. Lett., 93* (1982) 99; (e) B. R. McGarvey, *Transition Met. Chem. (N.Y.), 3* (1966) 89.
22 C. E. Bannister, J. M. Raycheba and D. W. Margerum, *Inorg. Chem., 21* (1982) 1006, and refs. therein.
23 J. Gelles, D. F. Blari and S. I. Chan, *Biochimica Biophysica Acta, 853* (1986) 205.
24 D. Kovacs and R. E. Shepherd, *J. Inorg. Biochem., 10* (1979) 67.
25 T. J. Lomis, M. G. Elliott, S. Siddiqui, M. Moyer, R. R. Koepsel and R. E. Shepherd, *Inorg. Chem.,* (1988), submitted for publication.
26 H. Kurosaki, H. Anan and E. Kimura, *Nippon Kagaku Kaishi,* (1988) 691.
27 J. C. Dabrowiak, F. T. Greenway, F. S. Santillo, S. T. Crooke and J. M. Essery, *ACS Symp. Ser., 140* (1980) 237.
28 R. G. Wilkins, *The Study of Kinetics and Mechanism of Reactions of Transition Metal Complexes,* Allyn and Bacon, Boston, 1974, pp. 198–201.
29 T. J. Lomis, J. F. Siuda and R. E. Shepherd, *J. Chem. Soc., Chem. Commun.,* (1987) 290.
30 M. Tsukayama, C. R. Randall, F. S. Santillo and J. C. Dabrowiak, *J. Am. Chem. Soc., 103* (1981) 458.
31 (a) M. F. Hoq and R. E. Shepherd, *Inorg. Chem., 23* (1984) 1851; (b) C. R. Johnson, W. W. Henderson and R. E. Shepherd, *Inorg. Chem., 23* (1984) 2754; (c) C. R. Johnson, R. E. Shepherd, B. Marr, S. O'Donnell and W. Dressick, *J. Am. Chem. Soc., 102* (1980) 6227.
32 J. A. Winter, D. Caruso and R. E. Shepherd, *Inorg. Chem., 27* (1987) 1086.
33 E. G. Janzen, *Acc. Chem. Res., 4* (1971) 31.
34 C. A. Evans, *Aldrichim. Acta, 12* (1979) 23.
35 R. K. Myser and R E. Shepherd, *Inorg. Chem., 26* (1987) 1544.
36 C. R. Johnson and R. E. Shepherd, in D. B. Rohrbacher and J. F. Endicott (eds.), *Mechanistic Aspects of Inorganic Chemistry,* ACS Symposium Series 198, American Chemical Society, Washington, DC, 1982.
37 C. R. Johnson, T. K. Myser and R. E. Shepherd, *Inorg. Chem., 27* (1988) 1089.
38 (a) A. Kittaka, Y. Sugano, M. Otsuka, M. Ohno, Y. Sugiura and H. Umezawa, *Tetrahedron Lett., 27* (1986) 3631; (b) M. Otsuka, A. Kittaka, M. Ohno, T. Suzuki, J. Kuwahara, Y. Sugiura and H. Umezawa, *Tetrahedron Lett., 27* (1986) 3639.